IMPROVING SENSITIVITY OF BIOSENSORS BY USING MICRO/NANO MAGNETIC PARTICLES

A THESIS
SUBMITTED TO THE DEPARTMENT OF ELECTRICAL AND COMPUTER ENGINEERING AND THE GRADUATE SCHOOL OF NATURAL SCIENCES OF ABDULLAH GUL UNIVERSITY
IN PARTIAL FULFILLMENT OF THE REQUIREMENTS
FOR THE DEGREE OF
MASTER OF SCIENCE

By
Omary MZAVA
August 2016

SCIENTIFIC ETHICS COMPLIANCE

I hereby declare that all information in this document has been obtained in accordance with academic rules and ethical conduct. I also declare that, as required by these rules and conduct, I have fully cited and referenced all materials and results that are not original to this work.

Name-Surname: Omary MZAVA

REGULATORY COMPLIANCE

M.Sc. thesis titled Improving Sensitivity of Biosensors by Using Micro/Nano Magnetic Particles has been prepared in accordance with the Thesis Writing Guidelines of the Abdullah Gül University, Graduate School of Engineering & Science.

Prepared By	Advisor
Omary MZAVA	Assist. Prof. Kutay İÇÖZ

Head of the Electrical and Computer Engineering Program
Assoc. Prof. Vehbi Çağrı GÜNGÖR

ACCEPTANCE AND APPROVAL

M.Sc. thesis titled Improving Sensitivity of Biosensors by Using Micro/Nano Magnetic Particles and prepared by Omary MZAVA has been accepted by the jury in the Electrical and Computer Engineering Graduate Program at Abdullah Gül University, Graduate School of Engineering & Science.

03 /08 / 2016

JURY:

Advisor : Assist. Prof. Kutay İÇÖZ ……

Member : Assist. Prof. Günyaz ABLAY ……

Member : Prof. Mustafa TÜRKMEN ……

APPROVAL:

The acceptance of this M.Sc. thesis has been approved by the decision of the Abdullah Gül University, Graduate School of Engineering & Science, Executive Board dated ……./……./2016 and numbered ……..……. .

……./……./2016

Graduate School Dean
Prof. Dr. İrfan ALAN

ABSTRACT

IMPROVING SENSITIVITY OF BIOSENSORS BY USING MICRO/NANO MAGNETIC-PARTICLES

Currently micro/nanoparticles such as magnetic beads are not only used as labels to acquire signals from biosensors but they are also used to enhance the signals obtained from various biosensors. Magnetic beads or target are linked to other molecular labels such as fluorescence and chemiluminescence labels by biomolecules such as antibody to reach higher sensitivity and provide signal amplification for the measurement. This dependency on biomolecular binding has several disadvantages such as molecular binding is sensitive to environmental conditions such as pH and temperature, labels are costly and molecular binding may require extra time.

In this thesis a time and cost efficient signal amplification method that does not need any biomolecular coating but based on magnetic interaction of magnetic micro/nanoparticles is developed. Magnetic particles subjected to external magnetic field are magnetized and form a local field around them, attract each other and accumulate along the magnetic field lines. These controlled accumulations can be used to amplify the pixel area or the contrast of magnetic particles. Accumulation dynamics of magnetic particles under magnetic field are studied and the application of this method to the Escherichia coli 0157:H7 sample is demonstrated.

Lastly the integration of this signal amplification method to a flow chamber and a complete biosensing procedure is pursued. Magnetic micro/ nano particles that are immobilized on gold-coated surface under external magnetic field inside a flow chamber attract the iron nanoparticles in a running fluid to form chains of accumulations around them. The accumulations formed under magnetic field are used to improve the Contrast to Noise Ratio (CNR) of the images thus the sensitivity.

Omary Mzava

Master's program in Electrical and Computer Engineering Department

Supervisor: Assist. Prof. Kutay İÇÖZ

August 2016

Key words: magnetic micro/nanoparticle accumulation, signal amplification, flow chamber, magnetic dipole-dipole interaction, biosensor.

ÖZET
MİKRO/NANO MANYETİK PARÇACIKLARI KULLANARAK BİYOSENSÖRLERİN HASSASİYETİNİ İYİLEŞTİRME

Halihazırda, manyetik boncuklar gibi mikro/nano parçacıklar sadece biyosensörlerden sinyal elde etmek için değil, aynı zamanda biyosensörlerden elde edilen sinyalleri güçlendirmek için de kullanılmaktadır. Hem algılama hem de işaret artırımı için çoğunlukla antikor-antijen bağlanması gibi biyomoleküllerin etkileşimi esasına dayalı bağlanmalar kullanılır. Bu biyomoleküler bağlanma olayı bir çok dezavantaja sahiptir. Biyomoleküler bağlanma pH ve sıcaklık gibi ortam şartlarına karşı hassastır, bağlanma için kullanılan etiketler pahalıdır ve moleküler bağlanma fazla zaman alabilir.

Bu tez çalışmasında, manyetik mikro/nano parçacıkların manyetik etkileşimine dayandırılan ve hiçbir biyomoleküler kaplama gerektirmeyen kısa sürede ve düşük maliyetli sinyal kuvvetlendirme yöntemi geliştirilmiştir. Dış manyetik alana maruz bırakılan manyetik parçacıklar manyetize olurlar ve bu parçacıklar etraflarında bölgesel bir manyetik alan oluşturarak, birbirlerini çekerler. Bu kontrol edilebilen manyetik etkileşim ve topaklanma, optik mikroskoplar ile elde edilen görüntülerdeki piksel alanının veya renk kontrastının yoğunluğundaki değişimler ölçülerek analiz edilebilir. Manyetik alan altındaki manyetik parçacıkların topaklanma dinamikleri teorik ve deneysel olarak irdelenmiştir ve bu yöntemin Escherichia Coli 0157:H7 bakterisine bağlanmış manyetik boncuklara uygulaması gösterilmiştir.

Son olarak, bu sinyal kuvvetlendirme yöntemi akış kanalıyla birleştirilmiş ve model hedef protein olarak streptavidinin algılanması gösterilmiştir. Akış kanalı içerisindeki altın yüzey üzerine sabitlenmiş mikro/nano parçacıklar, bu sıvı içerisinde hareket eden demir parçacıkları zincir şeklinde toplar. Manyetik alanda oluşturulan bu topaklanmalar görüntülerin Kontrast Gürültü Oranını artırmak için kullanılır ve böylece elde edilen işaret 6-8 kat artırılır.

Omary Mzava
Elektrik ve Bilgisayar Mühendisliği Ana Bilim Dalı, Yüksek Lisans Programı
Tez Yöneticisi: Yrd. Doç. Dr. Kutay İÇÖZ
Ağustos 2016

Anahtar kelimeler: Manyetik mikro/nano parçacıklar toplanma, işaret küvvetlendirme, akış kanalı, miknatis dipol-dipol etkileşimi, biyosensöler.

Acknowledgement

I would like to express my sincere gratitude and appreciation to my advisor Dr. Kutay İÇÖZ. Throughout the two years of my studies you have been a great mentor to me. I would like to thank you for believing in me and letting me work in your project. The discussions and suggestions you always give have played a great part towards the completion of this work. Also I would like to thank the members of the jury Dr. Günyaz Ablay, Dr. Mehmet Çağrı Soylu, Dr. Mustafa Türkmen, Dr. İsa Yıldırım for agreeing to take part in my thesis defense.

I would to acknowledge THE SCIENTIFIC AND TECHNOLOGICAL RESEARCH COUNCIL OF TURKEY (TÜBİTAK)-BIDEB 2215 SCHOLARSHIP PROGRAM for supporting my masters' degree studies. I would also like to acknowledge the support from TÜBİTAK (Project No: 114E886) and AGU BAP (2015-11).

My gratitude also goes to my fellow BioMINDS labmate Zehra Taş, who we have been working in the same project and has contributed heavily in part of this work. Your hard working spirit has always pushed me to work hard to keep up with the demands of the project. I will also like to acknowledge all other people who played a role towards the completion of this study which have not being mentioned here.

Lastly I would like to express my deepest gratitude to my mother and my younger sister for the endless prayers and support. I am thankful not only for always being there for me when I need them but for the great and strong people that you are.

Biography

Omary Mzava was born in 1989 in Kilimanjaro, Tanzania. After completing his primary school studies he joined Majengo secondary school and Ilboru secondary school for ordinary level and advanced level education respectively. He joined Selçuk University of Turkey under scholarship in 2010. He graduated from the Department of Electrical and Electronics Engineering in 2014 ranking the third best student in his class. After graduating he was selected among the recipients of the TÜBİTAK-BIDEB 2215 scholarship and joined Abdullah Gül University to pursue his Masters of Science in Electrical and Computer Engineering degree. During his graduate studies he worked on a TUBİTAK funded project as a research assistant. His research interests are microfabrication, BioMEMS and microfluidics.

Publication

Mzava O, Taş Z, İçöz K. Magnetic micro/nanoparticle flocculation-based signal amplification for biosensing. *Int J Nanomedicine*. 2016;11:2619-2631. doi:10.2147/IJN.S108692.

TABLE OF CONTENTS

LIST OF FIGURES

LIST OF TABLES

To My Father
You will always be remembered.

Chapter 1

Introduction

This chapter is dedicated to provide the background information that this work is built upon. The concept of Biosensors, its characteristics, components, and its types together with applications will be introduced. Later on Magnetic beads as applied in the field of biosensors will be reviewed as well. The magnetic properties of materials, synthesis of magnetic beads, different methods that are employed in the detection of magnetic beads together with the application of magnetic beads are briefly reviewed in this chapter. Lastly the main problem solved in this work is introduced and other current solution methods are discussed.

Biosensors are defined as analytical devices that incorporates biologically active elements with a suitable physical transducer capable of producing a measurable signal that is proportional to the concentration on the analyte of interest [1,3]. Analytes of interest may range from small proteins to large cells. An analyte as used in this context, is the compound whose concentration is to be determined. Research in this field dates as far back as in 1950's when Clark and Lyon introduced the first generation of Glucose biosensor [4] which serves as a blue print for the widely used modern day biosensors . Only two components are mentioned in the above definition but mainly biosensors contain three essential components. Namely: (1) probe (detector/bio receptor), (2) transducer and (3) signal processor Figure 1.1.

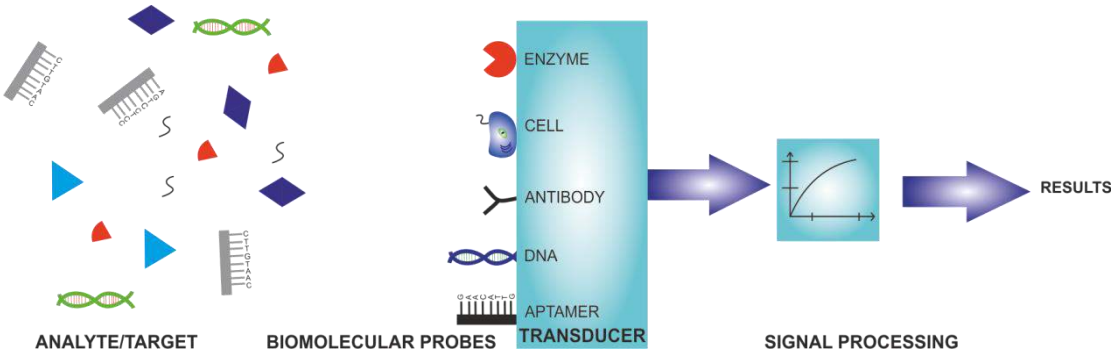

Figure 1.1 Illustration of the components of biosensors

Probe contains the immobilized biomolecules that recognizes (interacts) a specific analyte of interest. Examples of biomolecules that are used as probes include aptamers,

antibodies, extracellular matrix proteins, enzymes, DNA, cell receptors, microorganisms etc. The Transducer however, it's main function is to convert this biological phenomenon of interaction between bio receptor and the analyte into a measurable signal that is directly or inversely related to the analyte's concentration. The measurable signal in this case might be an electrical signal, optical signal, magnetic, electrochemical signal etc. This transduction is not only limited to one type of measurable signal. It might be a combination of the signals depending on the system design [5]. The last component contains signal processing unit that might integrate the necessary electronics and a display, to filter, amplify and perform further post processing to display the results in a user friendly way.

Most of clinical methods that are used in diagnosis and monitoring of diseases have proven to be costly in terms of both financially and time wisely, they also require specialized personnel and high volume of samples [3]. Biosensors are quite promising in this case since they require low volume of samples, they can be made with high specificity, they have fast response, low cost, they don't require specialized personnel and they can also be used to measure non polar molecules which do not respond to most measurement systems [6].

1.1 Types of Biosensors

In literature biosensors have been classified as either according to the biomolecular probe they use or the type of signal transduction mechanism that is employed. These categories together with their subcategories are shown in Figure 1.1.1. A brief introduction on some of them is explained below.

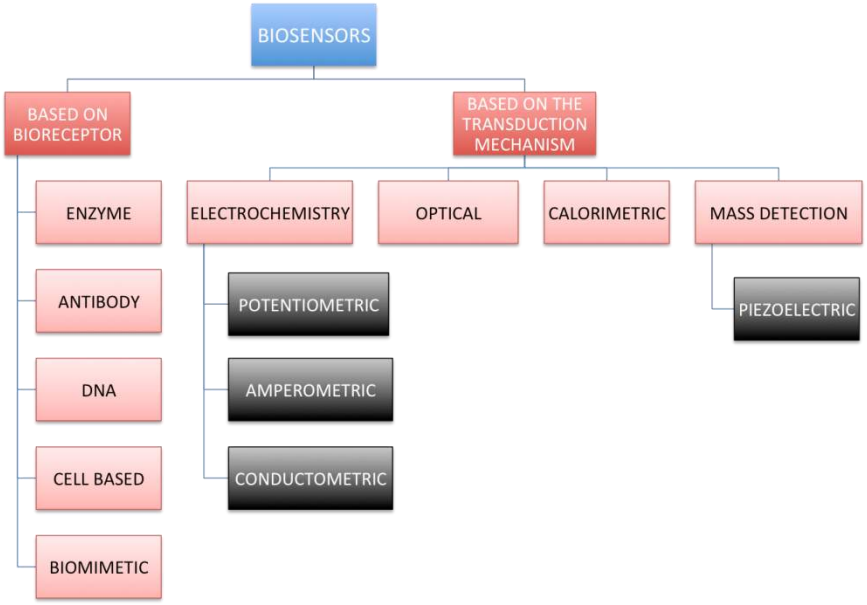

Figure 1.1.1 Classification of biosensors

1.1.1 Based on Transduction Mechanism

Signal transduction forms can be grouped in three broad categories. Namely: 1) Electrochemical detection mechanism 2) Optical detection mechanism and 3) Mass detection mechanism. The combination of these can also be achieved thus providing a wider range of possibilities.

Electrochemical Biosensors

The first of the devices that use this transduction method was reported in the work [4]. Where only the detection of glucose was conducted. Following this, there have been numerous improvements and added functionality on different biosensors that employ this method. Authors of [7] have developed a biosensor to monitor chemotherapy drugs and determine their damage or modification in the DNA. The working principle of sensors that fall under this category is the bio electrochemical reaction between the immobilized biomolecules and the target analyte will result in the production of electrons/ions which affects the electrical properties of the medium [8][9]. This change of the electrical properties (voltage/current) is correlated to the amount of the analyte that is present in the sample medium. This method uses potentiometry, amperometry and voltammetry techniques which gives further subclasses according to the signal measured.

Amperometric Biosensors, measure the current value of current density change

produced from an electrochemical reaction of an electrochemically active analyte at a constant applied potential voltage [10]. They are well known for their fast measurements, sensitivity and ability to measure analytes in opaque medium. In [11] , an amperometric biosensor that measures the concentrations of the combustible gases (hydrogen, carbon monoxide and methane) in the nitrogen atmospheres. The limiting current change was characterized at an operating temperature of 450°C. Adapting this sensor to other gases, it can be used for environmental monitoring of different pollutants.

Potentiometric biosensors, work under the condition of zero current flow in the electrodes, they measure the potential (electromotive force) that is produced by the reaction between an analyte and the electrode's membrane or surface. The potential generated is proportional to the logarithm of the electrochemically active analyte's concentration [12] and is compared to a reference potential.

The last subclass is conductometric biosensors, which measure the conductance/resistivity property of the medium when an electrochemical reaction occurs. This property is directly correlated to the amount of analyte present. Compared to other electrochemical biosensors, conductometric biosensors are considered to be more beneficial. They can be industrially produced at low cost, they can be miniaturized and highly integrated using inexpensive thin film standard technology to mention a few [13].

Optical Biosensors

The reaction between the analyte and the biomolecular probe on the surface of biosensor causes the change in absorbance or florescence that results from the change of the surfaces refractive index. Different parameters can be measured in this case, such as phase shift, polarization, energy, decay time and amplitude. However amplitude is used in most cases as it can easily be associated with the concentration of the analyte [14]. Also Surface Plasmon Resonance (SPR) Biosensors fall under this category.

Calorimetric Biosensors

These are the type of sensors that measure the amount of heat generated in an enzymatic reaction. The substrate of the enzyme is the analyte itself. These types of sensors include temperature sensors (thermistors) that convert heat into electrical signal.

The entire sensor is normally well insulated to ensure no heat loss is observed.

Authors of [15] have reported a calorimetric biosensor that is used to detect a poisonous Organophosphates (OP) in foods that's can cause serious effects to human beings. An enzymatic reaction between OP and chicken liver esterase catalyst used as probe generates heat that is used to determine the concentration of OP by comparing the temperature produced and the temperature before inhibition.

Mass Detection Based Biosensors

These types of biosensors are coupled with piezoelectric crystals. The surface of a piezoelectric material is made chemically active (functionalized) by probe molecules (e.g antibody) and made to resonate at a specific frequency by the application of an electrical signal. When an analyte is introduced and captured by the probe molecule there will be a change in the resonant frequency of the piezoelectric device [16]. This change is associated to the amount of the analyte captured. They are among the most sensitive biosensors used today.

1.1.2 Biosensors Based on Biomolecular Probes

Enzyme Based Biosensors

The first biosensor that was introduced by Clark and Lyons [4] was comprised of an amperometric enzyme electrode used in the detection of Glucose. Following this, enzyme based biosensors are more popular due to their specificities. As biocatalysts, enzymes can specifically bind to their substrate (analyte in this case) and catalyze them. Enzyme based biosensors rely on this property of specificity of the enzyme. Enzyme bioreceptors detects targeted analyte from a sample. This catalytic event can be observed as a change of the medium property (e.g temperature) and correlated directly to the amount of the analyte present.

Immunosensors

Application of antibodies based biosensors was first applied in the 1950s, thus opening doors to immune-diagnosis [17]. The requirement of high stabilility, specificity and versatile biosensors have led researchers to apply the natural occurring phenomena

of antibody-antigen binding in biosensors designing. Antibody binds specifically to its antigen and this event can be transduced either optically, electrochemically etc.

DNA Based Biosensors

This type of biosensors uses the high specificity binding property of DNA where two single stranded DNA (ssDNA) binds together to form one double strand (dsDNA). They work on the mechanism that an immobilized base ssDNA is used to capture its complementary target ssDNA in the sample and form a stable hydrogen bond comprising dsDNA. The transduction of this event can lead to different signals according to the system design.

Cell Based Biosensors

The working principle of this type of biosensor is that they rely on the ability of living cells (used as bioreceptors) to detect biochemical effects directly and transduce them into a measurable signal [18]. Some of the setbacks observed in this type of biosensors are the detection limit of cell based biosensors is mainly dependent on the medium condition that determine how long the cell can stay alive and stability of the cell that depends on factors like sterilization, biocompatibility and lifetime. However cell based biosensors are less sensitive and are tolerant to worse environmental conditions than enzyme based biosensors [17].

Biomimetic Biosensors

These biosensors contain an artificially manufactured bioreceptor that mimics the functions of natural bioreceptors. They are known as aptasensors, which use aptamers as bioreceptors. Aptamers are single stranded nucleic acids that can be used to detect different molecules such as proteins. These sensors' popularity is mainly due to their specificity, modification, immobilization versatility and structural change [17].

1.1.3 Application of Biosensors

Biosensors have widely been used in different fields. Their popularity is due to the fact that they provide better stability, high sensitivity and applicability than common current standards. Not only in research but currently different there are a number of

biosensors available in the market, drugstore and different medical shopping centers. They are widely used in medical field, Food safety and quality control (analysis), environmental monitoring and in biodefence. In the following sections these applications are explained and few examples are cited.

Food Analysis

Food Industry is a very important sector, requires suitable and reliable methods for analysis. Different contaminants are bad to the human health. Biosensors have been utilized checking and quantifying contaminants in foods [19]. However monitoring the quality of food is an important aspect also where biosensors have been utilized. Chemicals such sugars, amino acids, alcohols, sweeteners and others are among the food chemicals needing to be monitored. In fermentation process also, biosensors are applied to monitor sugars such as fructose and sucrose.

For example, there is a wide usage of antibiotics in dairy farming. The remainder of these antibiotics in the dairy products pose a great danger to the human healths thus it is of huge importance to monitor these levels. The authors in [20] have developed a biosensor to detect the amount of benzylpenicillin in milk.

Medical Application

Currently the clinical standards used in diagnosis and monitoring of diseases have proven to be laborious requiring high sample volumes, too much time, expertise and immobility. However Biosensors possessing several features such as low cost, high sensitivity, suitability for point of care diagnosis and other pose to be a great relief in clinical analysis and monitoring of different diseases. According to [21] more than 422 million adults were living with diabetes. Glucose biosensors have achieved great popularity today in the market as they form part of an essential component in managing diabetes.

Pregnancy testing forms another application where biosensors are widely used to detect the human chorionic gonadotrophin (hCG) hormone that is secreted during pregnancy.

Biosensors have also been used in the detection of cancer and cardiac biomarkers, different hormones, bacteria, virus and cancers cells as shown in [22,26].

Biodefence

The rate of terror crimes has been increasing very fast lately, it is logical to be ready for such evil acts as biowarfare. Biosensors can be used in real time monitoring the threats of biowarfare agents (BWA) such as bacteria, spores and viruses. Current developments in biosensor technologies have even improved more the real time detection and monitoring of BWA. Most sensors rely on the antibody antigen capturing property for quantification of BWAs. For example authors in [27] and [28] have designed biosensors for different anthrax biomarkers. Apart from different ongoing researches there are biosensors already in the market for the detection of these biothreats.

Environmental Monitoring

Several factors such as economic and industrial growth in the world have caused the increase in environmental pollution. Heavy metals, synthetic chemicals and pesticides are among the major contributors to environmental pollution. Biosensors are utilized to detect and quantify these pollutants [29].

1.2 Magnetic Beads

Magnetic beads have proven to offer attractive possibilities in different biomedicine applications. They possess different features that make them to stand out among other mainstream micro/ nanoparticles. Some of those features are: 1) they can be manufactured/synthesized at different sizes ranging from nanometer to micrometer scale as well as being coated by different coatings e.g. polymer making them non-toxic. Depending on where they are applied this size flexibility is an important factor. Taking an example the size of a cell ranging from (10 nm to 100 μm), magnetic beads can be made to this size or even less, making them easy to reach or get close to the cells. Biocompatibility is also an important feature if the beads are to be used in invivo applications. 2) They are magnetic, meaning they can be controlled/ manipulated by an externally applied magnetic field. This property has proven to be useful in cases that magnetic particles are used in non-magnetic background medium e.g. in blood since the blood is non-magnetic. In this way they can be moved and stopped, opening doors for different biomedical applications. 3) They can be made to respond to an externally

applied varying magnetic field. Meaning energy can be transferred to the magnetic beads opening up to much more applications [30]. 4) They can be detected by a number of methods.

Different magnetic beads are available in the market today. While their structure can be as complex as having a number of iron oxide particles inside a sphere polymer coating or a sphere polymer coated with iron oxide, they can also be as simple as just a single bead inside a coating. The preferred coatings are normally polymer matrix or silica. These coatings can further be functionalized with different biomolecules and used as biomolecular probes in different binding events and detection applications. Most of the beads have iron oxide cores. Maghemite and Magnetite have been used more since they can easily be formed. Cobalt and Manganese oxides have more attracting magnetic properties but there are concerns about their toxicity making them less favorable as cores [31].

Several factors are known to have an influence in the magnetic properties of the beads. Namely; chemical composition of the beads, degree of defectiveness, size and shape of beads to mention a few. By controlling these factors one can control the extent of magnetization of the beads [32].

1.2.1 Magnetic Beads Synthesis, Encapsulation and Functionalization

There are a number of parameters that are of particular interest in the synthesis and functionalization of magnetic beads. For example, their size, stability and shape. Different methods of synthesis of the magnetic beads have been reported for different composition of the particles [33,36]. Such as iron oxides example maghemite and magnetite, ferromagnets such as $MnFe_2O_4$, pure metals such as iron and cobalt etc. Generally most of the methods for synthesis reported in literature can be classified in about four broad groups. Namely: co-precipitation, micro emulsion, thermal decomposition and hydrothermal synthesis [37].

Co-precipitation is the simplest and efficient method used in synthesis of iron oxides from the iron salts where bases are added to aqueous iron solutions. This method generally produces beads of the diameter sizes less than 50nm. The size depends on the ratio of the iron ions concentration, the reaction temperature and pH.

Emulsion is defined as a mixture of two or more immiscible liquids. When these liquids mix up one liquid is dispersed in another liquid. And droplets are formed which

are unstable and their size keeps on increasing with time. Microemulsion is defined as a thermodynamically stable emulsion with features that do not vary with time. Their features size averages less than 100nm in diameter [38]. This method has been used to synthesize different kinds of magnetic particle like gold-coated cobalt beads, metallic cobalt and cobalt/platinum alloys.

Thermal decomposition is defined as a chemical reaction/decomposition that is caused by heat. Magnetic particles can be synthesized by decomposing organometallic compounds in boiling solvents containing suitable stabilizing surfactants.

After synthesis comes an important step that is used to encapsulate these magnetic particles to make them chemically stable, offer them protection against corrosive agents as well as provide a platform for further functionalization of the magnetic particles for different purposes. This covering gives the magnetic nanoparticles a core and shell structure. Different strategies are employed in protecting and covering of magnetic particles such as silica coating, oxidation coating, polymer coating and precious metal coating.

Following this step is the functionalization step where the coated magnetic beads are functionalized with different molecules such as biomolecules, catalytically binding species or different drugs.

1.2.2 Magnetic Properties

Magnetism is a property of exerting repulsive or attractive force observed on some materials on other materials. Magnetic field is created when there is a movement of electrons in magnetic materials producing the field and magnetization effect within it [39]. When a magnetic material is placed under an external magnetic field strength $\boldsymbol{H}$ whose SI unit is Ampere-Turns per unit meter (A/m), individual atomic moments contributes individually to the overall response of that material in that field [39][30]. This response is termed as magnetic induction or magnetic flux density denoted by $\boldsymbol{B}$ whose SI units are Tesla (T) or weber/m^2. The CGS units of magnetic field strength and Magnetic induction are Oersted (Oe) and Gauss respectively.

Given in the equation below is the relationship between the applied external field and the response of the material under consideration called the permeability of the material (μ). The relationship is linear in the case where the material medium is free space thus we have permeability of free space μ_0. But it is not linear in most cases

involving other media. Since μ may be varying as a function of the applied magnetic field.

$$\boldsymbol{B} = \mu \boldsymbol{H} \quad \textbf{(1.2.2.1)}$$

$$\mu_0 = \frac{\boldsymbol{B}}{\boldsymbol{H}} \quad \textbf{(1.2.2.2)}$$

This discrepancy in linearity due to material difference is compensated upon by magnetization (***M***), which is obtained by the following equation.

$$\boldsymbol{M} = \frac{\boldsymbol{m}}{\boldsymbol{V}} \quad \textbf{(1.2.2.3)}$$

Where ***m*** is the magnet moment and ***V*** is the volume of the material. Leading to the final relationship given as;

$$\boldsymbol{B} = \mu_o(\boldsymbol{H} + \boldsymbol{M}) \quad \textbf{(1.2.2.1)}$$

The above equation holds true for all media. All materials exhibit magnetism to some point depending on their atomic structure and temperature. Some are weak while some are strong. This phenomenon is best described by volumetric magnetic susceptibility χ, given by the following equation.

$$\boldsymbol{M} = \chi \boldsymbol{H} \quad \textbf{(1.2.2.2)}$$

Magnetic susceptibility is dimensionless and it can be used to classify materials behavior under magnetic field. The materials with small magnetic susceptibility are said to be less magnetic and vice versa.

Some materials have ordered magnetic states even under no magnetic field. They are classified as ferromagnets, ferrimagnets and antiferrimagnets, the susceptibility of these materials depends not only in temperature but also in the applied magnetic field ***H*** giving rise to a characteristic ***B-H*** curve that shows the relationship between applied external field and the magnetization achieved. An application of external field in these materials causes the atomic dipoles to align according to that field. Upon remove of the field, the magnetization does not return to zero. This lagging gives the what's called the Hysteresis loop. Shown in the Figure 1.2.2.1 below is a B-H curve for ferromagnetic material.

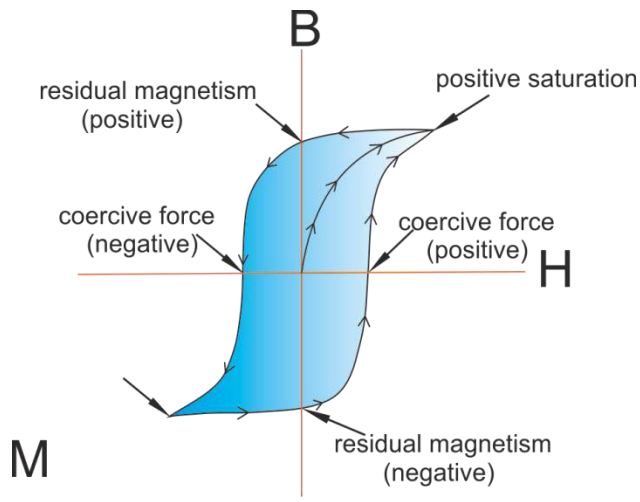

Figure 1.2.2.1 Ferromagnetic materials' B-H curve

Important points in the graphs are shown and defined. Magnetic saturation, this point is the highest magnetization achieved in the material any further increase in the field will not cause any effect. Remanence is the residual magnetism that is left behind upon the removal of the external magnetic field. Coercivity, is the magnetic field that is required to return the magnetization of the material to zero after saturation. This value gives a measure of the resistance of the material to become demagnetized.

1.2.3 Classification of Magnetic Materials

Magnetic materials are classified as explained in this section. The classes are ferromagnetic beads, antiferromagnetic beads, ferrimagnetic beads, paramagnetic beads and superparamagnetic beads.

Ferromagnetism

This phenomenon is observed in materials that can be attracted and can be made into magnets. Materials with this property are characterized by high magnetic permeability, high saturation point and hysteresis. In atomic level these material possess atomic moments that are aligned to each other in the regions called domains. In the regions there is magnetism but at this point but if the whole material is considered, there is no net magnetism because the domains themselves are all randomly aligned. Upon application of the magnetic field, the random domains align ordered and net magnetism is experienced.

They tend to keep their magnetization even after the removal of the external field. At high temperatures above the Curie temperature, the magnetization of the ferromagnetic materials disappears.

Ferrimagnetism

Materials possessing this property contain hysteresis loops which are similar to that of the above-mentioned ferromagnets (Figure 1.2.2.1). However small but ferromagnetic materials observe a permanent magnetic state. They have small susceptibility mainly due to the fact that these materials have net magnetization caused by the anti-paralleled and unequal magnetic moment of the coupled atoms in the material.

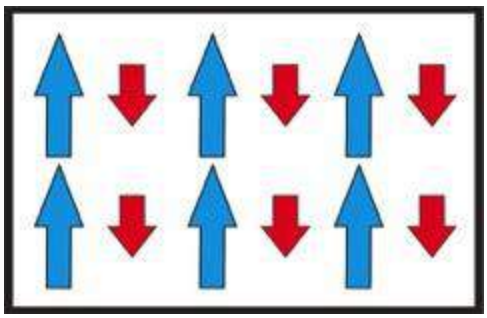

Figure 1.2.3.1 Magnetic moment alignment for ferrimagnetic materials

Antiferromagnetism

Materials that possess this kind of property have net zero magnetization. This is caused by the fact neighboring coupled atoms have equal in magnitude and anti-paralleled magnetic moments. They end up cancelling each other leading to net zero magnetization. Antiferromagnetic materials possess a very small negative susceptibility.

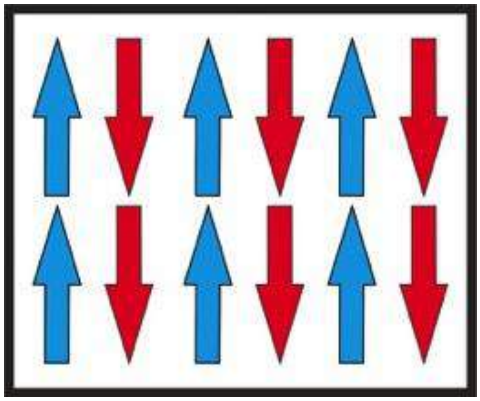

Figure 1.2.3.2 Magnetic moment alignment for antiferromagnetic materials

Paramagnetism

Paramagnetic materials temporarily observe weak magnetism and posses susceptibilities of the order of 10^{-6} to 10^{-1}. When the material is exposed to an external magnetic field, the atomic magnetic moments partially align up in the direction of the field and the material becomes weakly magnetized. Upon removal of the external magnetic field the material loses it magnetization immediately. The magnitude of the magnetic field induced is temperature dependent in paramagnetic materials. Thermal agitation limits the randomization within the atom, which limits the magnitude of the induced magnetic field.

Diamagnetism

This property is observed in materials that cannot be affected by magnetic field. Their atoms contain core electron in filled shells that resist any change to align electron spins upon application of magnetic field. The susceptibility of these materials is very small in the range of -10^{-6} to -10^{-3}. Meaning negative magnetization is achieved when these materials are subjected to an external magnetic field. They are repelled by magnetic field.

Superparamagnetism

This property is observed in smaller ferromagnetic and ferromagnetic beads [30][40]. The size can be as smaller as less than couple of tens of micrometer. They can be thought as having one giant magnetic moment composed of magnetic moments of atoms forming it. They are single domain magnetic beads. Their magnetic moment is free to flip randomly depending on the temperature while their individual atomic moments maintaining their original ordered state relative to one another. The average time between a flip is called Neel's relaxation time.

$$\tau = \tau_0 \exp\left(\frac{\Delta E}{k_B T}\right) \qquad \textbf{(1.2.3.1)}$$

Where τ is the relaxation time of the net magnetization of the particle τ_0 is the attempt time, ΔE is the energy barrier to moments reversal and $k_B T$ is the thermal energy. However the observation of superparamagnetism does not only depend on the

temperature and the energy barrier. In order to observe superparamagnetism measurements should be performed at a specific time called measurement time, τ_M.

Superparamegnetism depends on this measurement time. Two states may be observed from this situation. When the time between two flips is less than the measurement time ($\tau \ll \tau_M$), a superparamagnetic state is observed. And when the time between two flips is greater than the measurement time ($\tau \gg \tau_M$), a blocked state is observed.

Materials with this property have anhysteretic (no hysteresis loop) but sigmoidal ***M-H*** curve shown below [30]. When the magnetic field is removed their magnetization falls to zero.

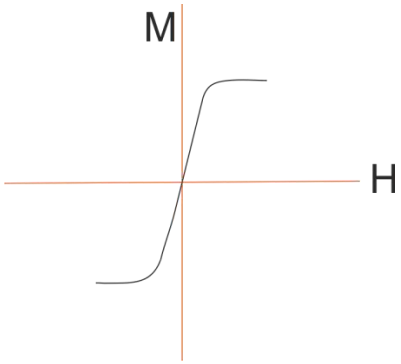

Figure 1.2.3.3 Superparamagnetic materials' M-H curve

1.2.4 Detection Methods for Magnetic Labels

The application and usage of magnetic materials in our daily lives have played an important role in developing magnetic beads detection methods for biosensors. Explained in the section are different ways that are used to detect magnetic beads or labels. The methods are grouped into two groups namely 1) Direct methods and 2) Indirect methods [41].

Direct Methods

Frequency Dependent Magnetometer

These devices works on the principle that, when a plastic strip containing super paramagnetic beads is placed inside a coil of an LC circuit, the resonant frequency of this circuit changes. The resonant frequency decreases as an assay containing magnetic

beads is placed between in the measuring coil. This decrease in resonant frequency is proportional to the number of magnetic beads present in an assay.

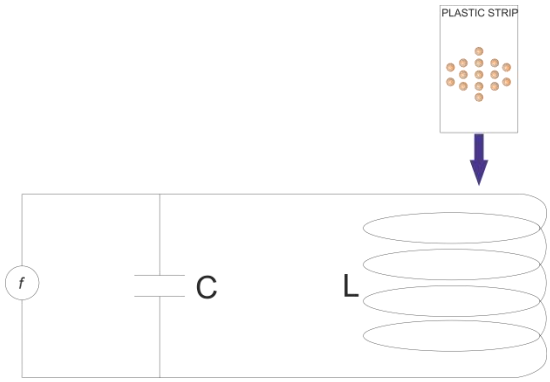

Figure 1.2.4.1 Illustration of frequency dependent magnetometer

Maxwell Bridge

One of the earliest methods to detect magnetic beads was through the measurement of magnetic permeability. In Maxwell bridge setup, the bridge is powered by a sinusoidal power source and any voltage variation is detected between point A and B. The inductor L_4 is used as a sensor for the magnetic labels/beads.

The bridge is firstly balanced at such that:

$$L_4 = R_2 R_3 C_1 \quad \textbf{(1.2.4.1)}$$

and

$$R4 = \frac{R_2 R_3}{R_1} \quad \textbf{(1.2.4.2)}$$

The inductance of the coil can be found by the following equation.

$$L = \frac{\mu_r \mu_o A N^2}{l} \quad \textbf{(1.2.4.3)}$$

Where R is the resistance, C is the capacitance μ_r is the relative permeability, μ_o is the permeability of free space, A is the cross sectional area of the coil, l is the length of the coil and N is the number of turns of the coil.

When a magnetic material (in this case the magnetic beads or label or a magnetic fluid) is introduced between the coils, it changes the permeability thus changing the inductance of the coil. This unbalances the whole bridge circuit and the change is observed in the output voltage across A and B. This output voltage is proportional to the number of magnetic beads.

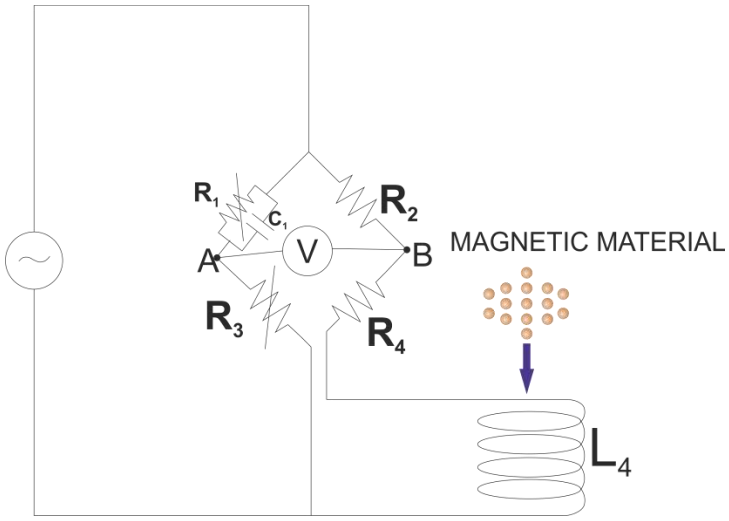

Figure 1.2.4.2 Maxwell's bridge setup

Superconducting Quantum Interface Device (SQUID)

This device forms one of the most sensitive and with high dynamic measuring range of all the magnetic field measurement technologies. It is used to detect the antibody coupled magnetic beads in a standard immunoassay. A sample containing the super paramagnetic beads is magnetized and al the beads are aligned in the magnetic field. This magnetic field is then removed; this removal leaves the magnetic beads aligned for a short period of time before randomizing again. This short event of keeping the magnetization is known as magnetic remanence. SQUID measures the decaying time known as Neel's relaxation time given in the equation below. Where τ_o is the excitation time, ΔE is the enrgy barrier, k is the boltzman constant and T is the temperature. The unbound magnetic beads decay very rapidly and do not have an effect on the measured time.

$$\tau_N = \tau_o \exp\left(\frac{\Delta E}{kT}\right) \quad \textbf{(1.2.4.4)}$$

Giant Magnetoresistance (GMR)

Magnetoresistance (MR) is a general name given to changes in materials' conductivity and resistivity upon application of magnetic field [42][43]. This effect is known to depend on the strength of the magnetic field and the direction of current. The sensitivity of the magneto resistive materials is given by the following equation:

$$MRratio = \frac{\Delta R}{R} = \frac{R - R_{Hsat}}{R_{Hsat}} \quad \textbf{(1.2.4.5)}$$

Where R_{Hsat} is the minimum resistance in saturation field. The following are some of the technologies that employ this property.

GMR is a quantum mechanics phenomena observed in thin film structures consisting of alternating layers of ferromagnetic and non-magnetic layers whereby a change in resistance is observed upon application of a magnetic field [44]. This effect was discovered by the authors of [45][46] in 1988 independently. They observed that this magnetoresistance change was greater than any other magnetoresistance change in metals observed before that's why this changes is called "Giant" magnetoresistance. When there is no magnetic field the magnetization in the ferromagnetic layers is antiparallel, upon application of magnetic field a parallel magnetization is obtained in the ferromagnetic layers causing a decrease in electrical resistance in the whole multi-layer structure. A magnetoresistance of 50% or more have been reported.

There are several types of GMR structures. The following are some of the structures as used in the detection of magnetic beads/particles.

Coupled Multilayer

This was the pioneering structure. Composed of alternating multi layers of ferromagnetic separated by a thin layer (about 1nm) of non-ferromagnetic layers shown in the figure below. There can be a couple stacks of layers. It employs the main working mechanism explained in the subsection 1.2.4.1.

Authors of [47] have created a biosensor system for capturing and detection of micron sized super paramagnetic beads on a chip containing an array of GMR sensors. The sensing mechanism involves ligand-receptor interaction and GMR sensing. The sensor's surface is patterned by a receptor molecule for certain target then a sample is passed. After capturing the target then magnetic beads coupled with a second set of receptor molecule allowed to attach on the sample that is immobilized on the sensor forming a sandwich structure. The super paramagnetic beads are now on the GMR sensor's surface. An external magnetic field is applied to the beads causing creation of a local field that is capable of producing a magnetoresistive change. The overall effect in resistance change is contributed by the resistance change caused by each magnetic bead.

Anisotropic Magnetoresistance

Anisotropic magnetoresistance effect occurs as a result of change in magnetization moment direction with respect to the current flowing in the material. Thus the resistivity of the material depends on the angle between the magnetic field and the electrical current in the material. Given by the following equation:

$$\rho = \rho_0 - \rho \cos\theta \qquad \textbf{(1.2.4.6)}$$

The anisotropic magnetoresistance ratio is given by the following equation.

$$AMR(\%) = \frac{\rho_{\parallel} - \rho_{\perp}}{\frac{1}{3}\rho_{\parallel} + \frac{2}{3}\rho_{\perp}} \times 100 \qquad \textbf{(1.2.4.7)}$$

Spin Valve

Spin valves works by using GMR magnetoresistive property although their structure are slightly different. In it's simple structure spin valves contain a layer of non-magnetic material sandwiched between ferromagnets. With one of the ferromagnets fixed (pinned) by an antiferromagnet whose purpose is to raise the coercivity and one left unpinned. The pinned behaves as a hard layer and the other as a soft layer. The difference in coercivity makes the polarities of the layers to respond to an applied magnetic field differently, with the free layer changing the polarity at lower fields. Two states can be achieved by this change in the free end's polarity. Parallel state which is a low resistance state and anti-parallel which is a high resistance state.

In [48], a GMR spin valve method for detecting magnetic nanoparticles (magnetic labels) showing a potential to be used in biodetection has been reported. Authors were able to detect magnetic nanoparticles from hundreds of them down to tens of them. The MR ratio in this case was around 11%.

Magnetic Tunnel Junction (MTJ)

Magnetic tunnel junctions are made of a non-magnetic metal layer sandwiched between ferromagnetic metals. The non-magnetic metal is made very thin so that electrons can tunnel from the magnetic metal upon application of bias voltage across the ferromagnetic layers. The tunneling current depends on the direction of the magnetic moment in the ferromagnetic layers. This orientation can be made to vary to parallel and anti-parallel thus producing high and low electrical resistance.

In [49], a Mg-O based MTJ biosensor is reported for detecting DNA. Mg-O based barriers as large as 200% MR ratios have been reported thus making them suitable for small magnetic field detection. The sensors contain 64 elements MTJ arrays functionalized with target DNA followed by the hybridization of the complementary target DNA. The magnetic beads coated with the probe DNA allowed to bind to the target forming the sandwich structure. The magnetic field responses curves were measured and plotted before and after binding of the magnetic beads. Clear differences were shown in the curves and signal to noise ratio analyzed. These differences suggested that Mg-O based MTJ biosensors hold promising capability in DNA or protein detection.

Silicon Hall Sensor

Discovered in 1879 [50] Hall effect is defined as the production of an electrical potential difference across a current carrying conductor when a magnetic field is applied externally perpendicular to the direction of flow of current. The potential difference created is due to the built up of charge carriers that are pushed by the magnetic field in the sides of the conductor. The direction of the potential difference is perpendicular to both electric current and the magnetic field's direction. The magnitude of this hall voltage is given by the following equation:

$$V_H = \frac{IH}{t} R_H \qquad \textbf{(1.2.4.8)}$$

Where V_H is the hall voltage created, I is the current flowing, H is the magnetic field strength, t is the thickness of the Hall region and R_H is the Hall coefficient.

Authors in [51] have reported a manufactured biosensor that is based in hall effect. It was manufactured using standard complementary metal oxide semiconductor (CMOS) manufacturing technologies. It was used to quantify magnetic beads bound to the sensor's surface, which gives the concentration of the analyte. Similar to ELISA the adhering of the magnetic beads on the surface is by immunological recognition thus requiring the beads to coated and functionalized.

Indirect Methods

Indirect detection of magnetic labels is done by exploiting the effect of the magnetic beads on the surrounding. This effect forms an indirect way of obtaining

information about the sample. Discussed under this section are some of the technologies employing indirect methods of detection.

Magnetic Relaxation Switches

Magnetic Relaxation switches work on the principle that involves the measuring the spin-spin relaxation time by using Nuclear Magnetic Resonance (NMR) technology. Detection of the target molecules involves measuring the relaxation times (T2) in the solution. Coated magnetic nanoparticles gathers to form clusters upon capturing the target molecules. This clustering causes the change in the relaxation time (T2) of the water protons [52]. The change in T2 provides quantitative data on the concentration and sensitivity[41]. This method however is more suited for detecting target molecules that are much smaller than the magnetic particles.

Microcantilever Based Force Amplified (FABS) Biological Sensor

FABS uses special type of cantilever made from piezoresistive materials that undergo a change in resistance upon application of mechanical stress. Antibodies to a known antigen are immobilized on the cantilever surface. When a target-containing sample allowed to flow on the cantilever's surface sample molecules are captured by the antibody antigen-binding event. After capturing the samples are labeled with antibody labeled magnetic beads to form a sandwich. An external magnetic field gradient in then applied, interacting with the magnetic beads on the cantilever's surface and causing it to bend due to the force experienced. This bending stress causes a change in resistance of the piezo micro-cantilever. The instrumentation coupled with cantilever allows the measuring of this change [53].

1.2.5 Application of Magnetic Beads

Targeted Drug Delivery

The goal of all drug delivery systems is to administer drugs specifically to targeted entities through medium that can control the delivery of the therapy by using a physical or chemical trigger. The extent in which this goal is achieved however is an issue since most chemotherapy methods are non-specific. Because intravenously administering of drugs leads to general distribution. The outcome of this is that drugs

that are aimed for the sick cells may also attack the healthy cells. Also the effect of the drug administered decreases even before reaching the targeted site/organ.

As a solution to this, researchers are pursuing the use of magnetic drug carries to deliver drugs only to specific area within the human body. The magnetic targeting method dates back to 1956 when researchers used injection method administered maghemite particles into the lymph nodes to selective induce heating after the surgical removed cancer (paper). The objectives of targeted therapy are as follows 1) to enhance drug targeting specificity 2) to lower the extent of drug toxicity 3) to improve treatment absorption rates 4) providing protection for pharmaceuticals against biochemical degradation (v) to reduce the amount of dose administered by target delivering.

Magnetically targeted therapy involves the attachment of the drug to a biocompatible magnetic particle. The drug/carrier complex is then administered by injection to the circulatory system of the patient. With the background medium being less magnetic, when the particles have entered the blood stream an external high gradient magnetic field is applied to move and stop the complexes to a specific site in the body. After concentrating the drug/carrier complexes at the target, the drug can be released by enzymatic activity or change in physiological conditions such as pH, temperature and be taken up by the tumor cells. By localizing the drug in only the diseased part, it is made possible to reduce the amount of dose of freely circulating drugs with small-targeted amount thus increasing the efficiency of the drug delivery.

The principle of magnetic targeting is based on the magnetic fields applied to the superparamagnetic particles resulting to a force that cause translational motion. The efficiency of this method depends on several factors like magnetic properties of the particle, the size and shape of the magnetic particles, field strength and also hydro dynamics parameters such as blood flow rate, concentration of the ferrofluids and also other physiological parameters such as distance of the targeted site from the magnetic field, strength of the drug/ carrier binding. Larger particles of the order 1μm have proven to be suitable for this purpose.

Biocompatibility and biodegradability is also an important issue if this process is to be adapted mainstream. Pure uncoated magnetic particles can not be used directly thus researchers are working on developing coatings that possess the two properties. The coating acts as a shield for the magnetic material and can be coated with other biomolecules.

Gene Delivery

This is the process of introducing a foreign DNA into a host cell for different purposes such as gene therapy. Gene therapy however can be defined as the introduction nucleic acids polymers to a patient's cell as a drug to treat a disease. Mostly DNA is used whereby a therapeutic gene is introduced and carried by a vector to replace a mutated gene. In gene delivery using magnetic particles the viral vector carrying the therapeutic gene is coated onto the magnetic carrier's surface. Then holding the carrier/vector complex at the targeted site using the external magnetic fields the virus is in contact with the tissue for a longer time thus increasing the efficiency of gene transfection and expression.

Hyperthermia

Hyperthermia in cancer treatment also called thermal therapy/thermotherapy is a type of cancer treatment in which a cancerous tissue is subjected to high temperatures of around 42-46 ℃ to kill the cancer cells [54]. Thermotherapy is divided into two, regional thermotherapy where the temperature of the part of the body (or the whole body) is raised to compliment other treatments such as chemotherapy and local hyperthermia where high temperatures are applied to a small area of cells. The former uses low temperatures than the latter. Since its invention numerous methods have been employed in thermotherapy. These methods involve the use of hot water, capacitive heating and inductive heating of malignant cells. However these methods all suffer a problem of localization and specificity, that it is difficult to heat the cancerous cells/tissue to the required temperatures without damaging the normal healthy surrounding cells.

In this method magnetic nanoparticles are spread on the targeted tissue and an AC magnetic field is applied. The AC applied should possess a strength that can cause the heating of the magnetic nanoparticles. This heat is transferred to the tissue and if maintained above the therapeutic limit for more than 30 minutes the cancerous tissue will be destroyed.

This method however faces two challenges: 1) delivering the amount of magnetic nanoparticles that can cause effective heating 2) using AC field strengths that are clinically safe. Enough heat must be generated to obtain 42 ℃ for about 30 minutes.

Calculating the heat deposition rate to achieve this is a challenging task since the presence of blood flow and tissue perfusion causes cooling of the tissue.

Physiological response to high magnetic frequency magnetic field such as stimulation of skeletal muscles, cardiac stimulation and non-specific inductive heating of tissues provide a limit on the frequency and strength of the externally applied magnetic field. The safe usable range is f=0.05-1.2MHz and H=0-15 kAm^{-1}.

The amount of magnetic nanoparticles required is dependent solely on the method of administration. Direct injection causes more concentration of the magnetic nanoparticles around the target tissue compared to other methods as antibody targeting. But each method has its own advantages and disadvantages. Mostly magnetite and maghemite particles that are smaller than 10 μm are used due to their biocompatibility and stability.

The Ferromagnetic particles possess a hysteretic property when exposed to AC magnetic field which gives rise to magnetic heating. The heat produced per unit volume is given by the frequency multiplied by the total area of the hysteresis loop. The formula ignores heating due to eddy currents since the magnetic nanoparticles are too small and the magnetic energy is too low to generate a considerable amount of eddy currents.

Magnetic Separation

Separation is a standard procedure that is used in the laboratories to ensure availability of concentrated samples or to separate biological entities from mass of samples or their native environment for further analysis [55].

Magnetic particles have proven to be useful in this case too. Application of magnetic particles for separation involves two steps. (i) Targeting and labeling of the needed biological entity using a magnetic label (tagging) (ii) separation of the labeled entities using magnetic separation based devices.

Targeting the biological entities is done by functionalized magnetic nanoparticles. A biocompatible polymer like dextran or Polyvinyl Alcohol first covers magnetic nanoparticles. This has an additional advantage that it increases the colloidal stability of the magnetic fluids. The specific binding sites on the surface of the cells are targeted using antibodies or other biological macromolecules like folic acid or hormones.

After tagging step the whole complex is passed in a magnetic separator. Magnetic separator provides the magnetic field gradient needed to separate the tagged entities

from their background solution. The magnetic force described later in the following chapter is used to immobilize the separated entities. This force has to be greater than the hydrodynamic drag force acting on the tagged material flowing in the solution.

The separator can be designed to be as simple as just a test tube and a magnet placed at the side or can be of a much more complicated design depending on the needs.

The magnet pulls the magnetically tagged cells/particles towards the wall and the remaining part can be poured away or removed. This process has proven to be slow. A different approach is employed to increase the efficiency as well as the accumulation rate. Creation of high magnetic field gradients regions within separator. This is achieved by placing a magnetizable matrix inside while the field is applied.. This can is much faster than the initial method. Another method is by using specifically designed field gradient system like quadropolar arrangement. Which creates a magnetic gradient radially outwards from the center of the flow column.

Contrast Enhancement Agent in MRI

Magnetic resonance imaging **(**MRI**)** relies on the magnetic moments that are produced by spinning protons. The effect is of the protons is huge in the presence of a steady magnetic field $\boldsymbol{B_o}$ since there are a lot of them in biological tissue. Hydrogen nuclei found in waters molecules inside a human body accounts for the images that can be taken using this method.

The basic idea is that the protons spin on their own axis and possessing a magnetic moment **M**. when a uniform external field $\boldsymbol{B_o}$ tuned to Lamor frequency ω_o is applied the spinning of the protons aligns parallel to the uniform field. This behavior is called Lamor Precession and is proportional to the magnetic field strength given as:

$$\omega_{o=}\gamma B_o \qquad \textbf{(1.2.5.1)}$$

Where γ is the gyro metric constant.

To obtain an image of the object, the object is placed inside a uniform field B_o and the hydrogen nuclei's spin align with this external uniform field and the net magnetic moment M in parallel to the field also.

Next a radio frequency pulse is applied which causes **M** to tilt away from $\boldsymbol{B_o}$. When the radio frequency is removed the nuclei realign themselves such that M is again parallel to $\boldsymbol{B_o}$. This process is known as relaxation. During this relaxation process nuclei lose energy by emitting their own RF signal. This signal is called Free Induction Decay

(FID) response signal. This response signal is picked up and measured by the inductive coils, and further the measurement is processed to obtain a grey scale image of the object.

The contrast/intensity of the tissue depends on the proton density and the longitudinal relaxation time T_1 and transverse relaxation time T_2. T_1 measures the time required for the displaced nuclei to return to equilibrium and T_2 measure the time for the FID response signal from a given tissue type to decay.

The contrast of the image obtained from MRI is a function of response signals from particular radio frequency pulses and depends on the factors that have been explained above. Super paramagnetic particles can change the rate at which the protons decay from their excited to equilibrium states. The biocompatible particles can be used in certain tissues by targeting them and produce a local field in application of the large external field. This results to shortening of the proton relaxation times thus changing the contrast of the image[56].

1.3 Problem Definition

Biofunctional micro/nanoparticles have proven to be a very important component towards attaining ultrasensitive level of detection and miniaturized assays. They can be used as tracers or carriers to obtain amplified signals or probes [57]. Magnetic particles as labels for signal amplification have been well explored in different works. To achieve signal amplification magnetic particles are linked to other molecular labels such as fluorescence labels [58], chemiluminescent labels [59] and quantum dots [60]. This linking is done by using a secondary non-magnetic label coated with a biomolecule (e.g antibody) binding itself to the magnetic particles or to the target molecule and provide signal or signal amplification. The signal obtained is correlated to the amount of the target molecules present in an assay.

The use of biomolecular binding events in assays however, has some setbacks. Firstly, binding events are very sensitive to the environmental conditions such as pH of the medium, temperature and ion concentrations. High care must be observed if high binding rates are to be achieved in this case. Secondly, the labels coated with biomolecules are expensive compared to the non-coated labels. And lastly, some of this reactions require extra time and specific buffer solutions for detection [14].

In this work a, novel magnetic particle based signal amplification method is reported. This method is not cost and time efficient, does not need temperature, pH control or specific buffer conditions and does not need any extra biomolecule such as fluorescent labels.

The mechanism of this method is as shown in the Figure 1.3.1 below. Primary magnetic beads capturing target molecules (referred as base beads in this work) are subjected under and external magnetic field. Upon magnetization of the base beads, they create a local force field around them. Other magnetic beads (uncoated) or iron nanoparticles are added (referred as added beads in this work). By dipole- dipole interaction the added beads are attracted to the base beads thus forming clusters/flocs/tails. This will be seen as an increase in area/ length of the base beads in the 2D camera images obtained, thus providing signal amplification.

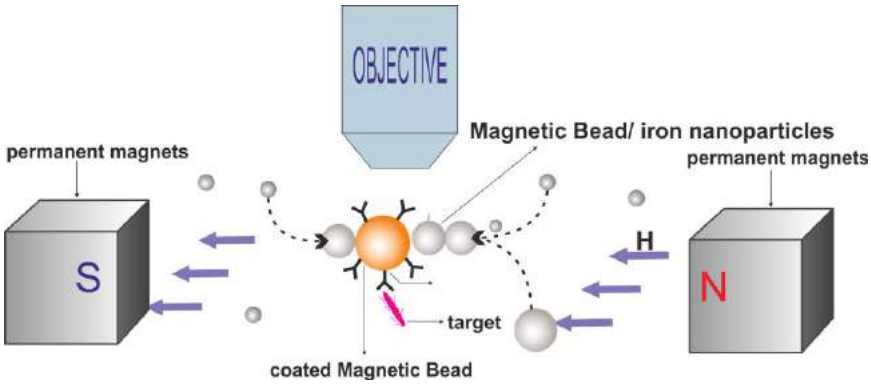

Figure 1.3.1 Demonstration of the experimental setup and magnetic beads accumulation based signal amplification

In this work the focus is aimed at studying the dynamics of this method for signal amplification, combination of this method with magnetic separation and the integration of this signal amplification method in flow chamber and surface functionalization. Lastly a complete biosensing method involving the detection of proteins (streptavidin) is demonstrated.

Chapter 2

Forces on Magnetic Particles in a Solution

The foundation of this work is mainly based on the forces that are experienced by magnetic particles inside a fluidic system and the interaction between these magnetic particles/ beads under these forces. A fluidic system in this case can be a drop or even a flow chamber. Magnetic beads can be controlled or manipulated by an external magnetic field. External magnetic fields are usually provided by electromagnets or using commercially available permanent magnets. They can all produce different ranges of magnetic field and forces depending on different parameters like the distance between the magnets and the magnetic beads or by controlling the current flowing through the coils of the electromagnets. This property is very useful in magnetic separator devices.

The controllability of the magnetic beads in any fluid system is dependent on several numbers of forces. Namely, magnetic force from all sources, drag force, gravity, particle-fluid interactions, inertia, Brownian motion, buoyancy and interparticle effects. These forces are reviewed in [61,63]. The dynamics of the magnetic beads in a microfluidic system can be modeled by the following equation as given in [61].

$$m_i \frac{d^2 x_i}{dt^2} = \boldsymbol{F}_{m,i} + \boldsymbol{F}_{D,i} + \boldsymbol{F}_{B,i}(t) + \sum_{\substack{j=i \\ j \neq i}}^{N} \left(\boldsymbol{F}_{dd,ij} + \boldsymbol{F}_{vdw,ij} + \boldsymbol{F}_{sur,ij} + \boldsymbol{F}_{hyd,ij} \right) \quad (i = 1, \dots, N) \tag{2.1}$$

Where m and $x_i(t)$ represents the mass and the position of the ith particle. The right side of the equation presents the forces on the ith particle. $F_{m,i}$ is the force due to an external magnetic field, $F_{D,i}$ is the drag force, $F_{B,i}(t)$ is the force accounting for Brownian motion. Interparticle interactions are modeled by the summation term. $F_{dd,ij}$ is the magnetic dipole-dipole force, $F_{vdw,ij}$ is the van der waals' force, $F_{sur,ij}$ is the repulsive force due to surfactants and $F_{hyd,ij}$ is the hydrodynamic force from interaction

of the particles. The inertia term helps to predict the motion of the particle with high precision at high acceleration.

The major emphasis is given in the dynamics of magnetic beads in low concentrated and slow moving fluids only the dominant forces are discussed and a special discussion is given on the interparticle forces (magnetic dipole-dipole forces) since they form a very important component of this work. These forces cause the magnetic beads to attract each other to form suprastructures in form of chains or flocs. When dealing with diluted magnetic solutions the interparticle effects can be neglected. Thermal kinetics (Brownian motion) are also ignored when the particle used are larger enough. The criterion for this is given in [64].

2.1 Magnetic Force on a Magnetic Bead

In manipulation of beads it is understood that uniform field will only give the magnetic beads a torque effect but to give a translational motion a magnetic field gradient is required [65]. The derivation of the magnetic force acting on the magnetic beads inside a magnetic field is shown below. The ultimate equation is given in literature but most of them do not show the derivation or references to the derivation making the user harder to decide how it is used in a certain experiment [66]. Magnetic force $\boldsymbol{F}_m$ acting on a point like magnetic dipole $\boldsymbol{m}$ is given from the derivative of the magnetic energy [67].

$$\boldsymbol{F_m} = \frac{1}{\mu_0}\nabla(\boldsymbol{m}\cdot\boldsymbol{B}) \tag{2.1.1}$$

where $\mu_0$is the permeability of vacuum. Another form of the equation is given as:

$$\boldsymbol{F_m} = \frac{1}{\mu_0}(\boldsymbol{m}\cdot\nabla)\boldsymbol{B} \tag{2.1.2}$$

This equation only holds when the magnetic moment of the particles is not varying in time (i.e.$\nabla\cdot\boldsymbol{m} = 0$) or the magnetic field is high enough to cause complete saturation of the magnetization. For the magnetic moment $\boldsymbol{m}$, it can be written as:

$$\boldsymbol{m} = V_m\mu_0\boldsymbol{M} \tag{2.1.3}$$

Where V_m is the volume of the particle and $\boldsymbol{M}$ is the magnetization of the particle. If the particle has a core and shell structure where the shell is polymer and diamagnetic then the volume of the core is used in this case. $\boldsymbol{M}$, is also given by,

$$\boldsymbol{M} = \Delta\chi\boldsymbol{H} \tag{2.1.4}$$

where $\Delta\chi$ is the relative susceptibility of the particle to the medium. If the medium is water then its given by :

$$\Delta\chi = \chi_m - \chi_w \tag{2.1.5}$$

Where χ_m is susceptibility of the magnetic particle and χ_w is the susceptibility of water. From Equation 1.2.2.1 the equation in Equation 2.1.1 simplifies to the final form below.

$$\boldsymbol{F}_m = \frac{V_m \Delta\chi}{\mu_0}(\boldsymbol{B}\cdot\nabla)\boldsymbol{B} \tag{2.1.6}$$

2.1.1 Accounting for Initial Magnetization

Magnetic beads are known to have complex structures depending on the manufacturing processes and design. Some of them have single core while other have multiple cores covered with coating of different materials such as silica and polymer. These structural complexities make it difficult to determine the exact magnetic moment ***m*** of the bead and its dependence on the magnetic field. However manufactures do provide the **B-H** response curves that make the work a bit easy. The authors of [66] have tried to model the motion of superparamagnetic beads in microfluidic channel based on the given conventional magnetic force equation above. But they found that the parameters given by the manufacturers could not match with the experimental data. To solve this problem it was necessary to modify the force equation to also account for the non-zero magnetization of the bead. They used magnetization and susceptibilities of the beads as parameters that can be adjusted. And the results they came up with were the model based on the corrected equation agreed well with the data.

The magnetization ***M*** of superparamagnetic bead varies approximately linearly with the applied magnetic field (weak fields) shown in the equation below. $\boldsymbol{M_0}$ represents the initial magnetization of the beads and ρ represents the density of the beads in SI unit. The initial magnetization of the bead is always parallel to the field and has a value ranging from 0 to a maximum of the remnant magnetization.

$$\boldsymbol{M} = \boldsymbol{M_0} + \frac{\chi_m}{\rho}\frac{\boldsymbol{B}}{\mu_0} \tag{2.1.1.1}$$

Ignoring the complexities of the beads' internal structure χ_m represents the susceptibility of the bead. This value is obtained by taking the average of the slopes in **M-H** curve given by the manufacturers. It is convenient to use the average value since the magnetic beads inside the same lot can have different values of susceptibilities.

$$\chi_m = \rho \frac{\Delta \boldsymbol{M}}{\Delta \boldsymbol{H}} \quad \textbf{(2.1.1.2)}$$

The magnetic moment $\boldsymbol{m}$ is given by the following equation:

$$\boldsymbol{m} = \rho V_m \boldsymbol{M} \quad \textbf{(2.1.1.3)}$$

Substituting M , we end up with the following equation:

$$m = \rho V_m \left(\boldsymbol{M_0} + \frac{\chi_m}{\rho} \frac{\boldsymbol{B}}{\mu_0} \right) \quad \textbf{(2.1.1.4)}$$

The above argument leads to the modification of the conventional force equation used to calculate the magnetic force experienced by the magnetic particles inside a magnetic field.

$$\boldsymbol{F_m} = (\boldsymbol{m} \cdot \nabla)\boldsymbol{B} \quad \textbf{(2.1.1.5)}$$

Leading to the final equation:

$$\boldsymbol{F}_m = \rho V_m (M_0 \cdot \nabla)\boldsymbol{B} + \frac{V_m \chi_m}{\mu_0} (\boldsymbol{B} \cdot \nabla)\boldsymbol{B} \quad \textbf{(2.1.1.6)}$$

Comparing to the conventional force equation in this equation there is an extra term caused by the initial magnetization. The conventional force equation in the does not account for the initial magnetization but however small it might be, in weak magnetic field the effect of the initial magnetization may be comparable to the effect caused by the weak external magnet. Ignoring this may lead to the deviation of the experimental parameters from the manufacturers' specification.

The magnetic force is normally provided by electromagnets or permanent magnets. Permanent magnets have an advantage of electromagnets in that they don't operate using a power source, they generate no heat and substantially magnetic force can be produced from permanent magnets.

2.2 Drag Force

For spherical particles the fluidic forces is estimated by using the Stokes' law. The major condition is that the flow should have a low Reynolds' number given by the Equation 2.2.1. Where η is the dynamic fluid viscosity of the suspending fluid, r_p is the radius of the particle and u_f being the velocity of the fluid and u_p the velocity of the particles.

$$\boldsymbol{F}_D = 6\pi\eta r_p(u_f - u_p) \tag{2.2.1}$$

The drag force opposes the net particle motion however in the cases which involve the movement of the magnetic beads by using magnetic force the drag force is comprised of two distinct forces. One of the forces opposes the movement caused by the fluid flow and the other opposes the movement caused by the magnetic forces.

2.3 Magnetic Bead-Bead Interaction

In this thesis the study of the nature of interaction between magnetic beads under external magnetic field is of huge importance since most of the experiments conducted in this work much depends and revolve around two relationships. 1) The relationship between the applied external field and the magnetic beads. 2) The relationship between magnetic beads under external applied magnetic field. Under external field the magnetic beads interaction can be treated as dipole-dipole interaction. This assumption is valid for the two magnetic beads with their distance of separation greater than their particle size. When two particles are considered, the magnetization on one particle causes magnetization on another particle. Depending on the position between the particles attractive and repulsive forces can arise [61] as well as torque can also be experienced. The torque will tend to be aligning the magnetic beads if they when they are not aligned. If the beads are assumed to be dipoles then the force caused by one bead on another bead under external magnetic field is derived below as discussed in [68] using the vector differentiation approach.

The magnetic field generated by magnetic dipole *a* at the position where magnetic dipole *b* is situated is given by:

$$\boldsymbol{B}_{ab} = \nabla \times \boldsymbol{A} \tag{2.3.1}$$

Where $\boldsymbol{A}$ is the magnetic dipole potential given by:

$$\boldsymbol{A} = \frac{\mu_0}{4\pi}\frac{\boldsymbol{m}_a \times \boldsymbol{r}}{r^4} \tag{2.3.2}$$

Substituting $\boldsymbol{A}$ and further calculating the field is obtained as:

$$B_{ab} = \frac{\mu_0}{4\pi}\left(\frac{3\boldsymbol{r}(\boldsymbol{m}_a \cdot \boldsymbol{r})}{r^5} - \frac{\boldsymbol{m}_a}{r^3}\right) \tag{2.3.3}$$

The force that is exerted by bead *a* on bead *b* is given as:

$$\boldsymbol{F}_{ab} = \nabla(\boldsymbol{B}_{ab} \cdot \boldsymbol{m}_b) = \frac{\mu_0}{4\pi}\nabla\left(\left(\frac{3\boldsymbol{r}(\boldsymbol{m}_a \cdot \boldsymbol{r})}{r^5} - \frac{\boldsymbol{m}_a}{r^3}\right) \cdot \boldsymbol{m}_b\right) \quad \textbf{(2.3.4)}$$

By manipulating the above equation, the final that is exerted by dipole *a* with magnetic moment $\boldsymbol{m}_a$ on dipole *b* with magnetic moment $\boldsymbol{m}_b$ separated with a distance vector **r** is given as follows.

$$\boldsymbol{F}_{ab} = \frac{3\mu_0}{4\pi r^5}\left[(\boldsymbol{m}_a \cdot \boldsymbol{m}_b)\boldsymbol{r} + (\boldsymbol{m}_a \cdot \boldsymbol{r})\boldsymbol{m}_b + (\boldsymbol{m}_b \cdot \boldsymbol{r})\boldsymbol{m}_a - \frac{5(\boldsymbol{m}_a \cdot \boldsymbol{r})(\boldsymbol{m}_b \cdot \boldsymbol{r})\boldsymbol{r}}{r^2}\right] \quad \textbf{(2.3.5)}$$

Considering two magnetic beads shown by the diagram below. The magnetic force between two beads can be decomposed to two components named the radial and tangential component. A general form of these forces are given in [69].

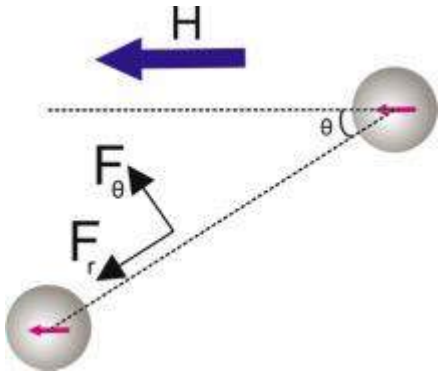

Figure 2.3.1 Diagram showing the positions of the interacting magnetic beads and the magnetic fields direction

The approximate polar equations of this force consisting of the radial force F_r and tangential force F_θ are given below. Where *R* is the distance between particle centers, *a* and *b* are the radius of the interacting particles, *B* is the magnetic flux density, μ_0 is the permeability of free space, χ is the magnetic susceptibility, and θ is the angle between the magnetic field direction and the line connecting the particles' centers. The Figure 2.3.1 shows the relative positions of the interacting magnetic beads inside an external field. The direction of the magnetic field is shown in arrows.

$$\boldsymbol{F}_r \approx -\frac{2\pi\chi^2\boldsymbol{B}^2a^3b^3}{3\mu_0\boldsymbol{R}^4}(1 + 3cos2\theta) \quad \textbf{(2.3.6)}$$

$$\boldsymbol{F}_\theta \approx -\frac{4\pi\chi^2\boldsymbol{B}^2a^3b^3}{3\mu_0\boldsymbol{R}^4}sin2\theta \quad \textbf{(2.3.7)}$$

The direction of the dipole-dipole force field is determined by the $1+3cos2\theta$ and $sin2\theta$ terms in equations 1 and 2, which coincide with the trajectories. Due to the $1/R^4$

term the forces F_r and F_θ increase significantly as the distance between the particles decreases. Different forms of the tangential and the radial components of force are also given in [69]. The dipole-dipole force field is drawn and depicted below in Figure 2.3.2 for the force on the second bead when placed at any point in the field. Depending on the position where the bead is situated the nature of the force can either be attractive of repulsive.

The force is attractive when the particle is placed at any point along the y-axis and repulsive when the particle is placed along the x-axis. At the position between both the x and y-axis, both the tangential and radial forces existt and seems to drive the beads to either the position where the attraction may occur or the position where the repulsion may occur.

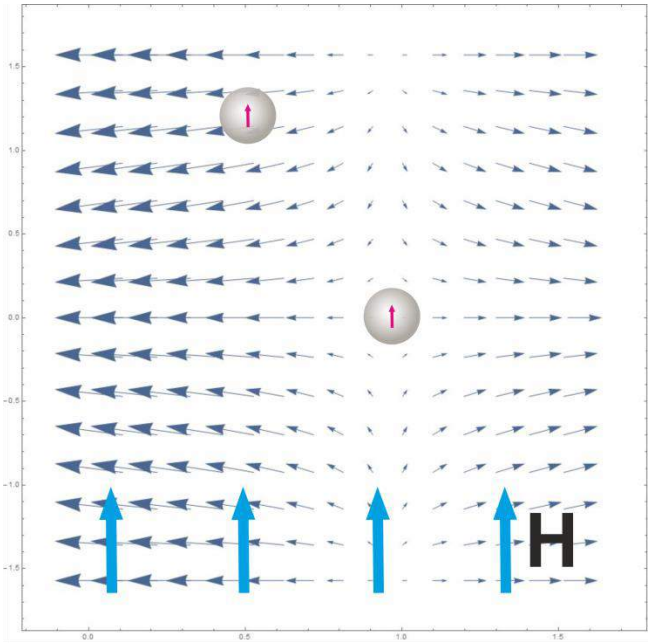

Figure 2.3.2 Normalized dipole-dipole force field

However this interaction does not hold for all magnetic materials. For soft magnetic materials the magnetization of one bead also affects the magnetization of the other particle and vice versa [69]. Thus the interaction force explained does not always account for the coupling force among soft magnetic materials.

Chapter 3

Magnetic Platform Design

To provide an optimum required magnetic field, a magnetic platform was needed. The main functions of this platform are two fold, 1) provide the main working area where the magnetic beads containing glass slide will be placed 2) holding the permanent magnets at the required positions to provide the necessary magnetic field. Thus designing a good magnetic platform forms an important part of this work.

The magnetic platforms are made from the PMMA material. The cutting and scanning are done using a laser cutter machine. Cutting named as vectoring and scanning is named as rastering in the laser cutting machine software. Vectoring cuts through the PMMA and rastering is only aimed to scan and dig the PMMA but not cut through. It is necessary to adjust the intensity of the laser so as to have the PMMA cut smoothly. Too much power of the laser will burn the platform and distort its clarity and transparency while too little intensity in the laser will not cut through the PMMA.

Also the cutting and scanning speed of the laser are important parameters as less speed will be a waste of energy and too much speed may fail to complete the cutting process.

The main working area is the place where the glass slides with magnetic beads on top of it could be placed on for magnetization and for viewing under the microscope. This place is designed taking into considerations the size of the glass slides and the position in relation to the permanent magnet.

The permanent magnets holding place is designed specifically to hold the permanent magnets in place and to contain enough area to accommodate a number of magnets on both sides of the working area. An adjustable number of magnets are needed in this area so as to provide the user with an option to vary the strength of the magnetic field that will be observed in the working area.

Other factors that has to be taken into account are that the magnetic field should be as uniform as possible in the working area so that much of the area of any drop containing glass chip placed on the working area will experience uniform field and a the global maximum of the magnetic field inside the platform to be as high as possible.

Three different designs were considered and simulated in FEMM software. One thing they have in common is that they were all designed for conveniently being placed under the microscope objective during the experiments.

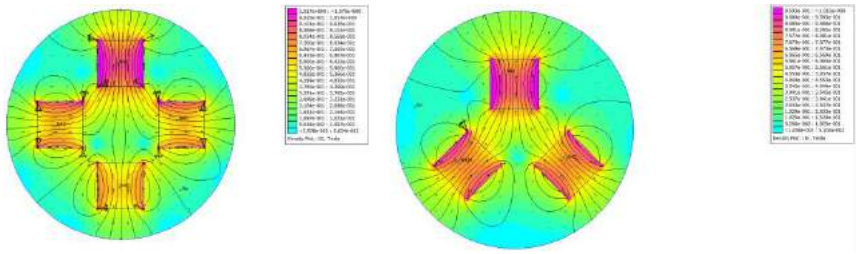

Figure 3.1 Magnetic field distribution maps for the proposed arrangement of permanent magnets

As shown in Figure 3.1, these designs were both simulated using FEMM software. The figures represent the magnetic field distribution in Tesla. The different permanent magnets' orientations were aimed at obtaining the one that will produce the highest magnetic field at the center for magnetization of the magnetic beads. With the separation distances the same, the vertical magnets design shown in Figure 3.2 produces the highest magnetic field at the center compared to the designs shown in Figure 3.1. The magnetic fields at the center for the designs in figure Figure 3.1were around 0.25 T and 0.5 T for the Figure 3.2.

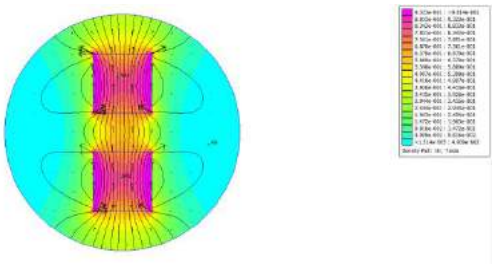

Figure 3.2 Magnetic field distribution map for the chosen permanent magnets arrangement

The vertical orientation of the magnets with opposite poles facing each other was chosen and implemented as shown Figure 3.2 since it is much simple to implement and produces higher magnetic field compared the others. This orientation of magnets was used for the remainder of this work.

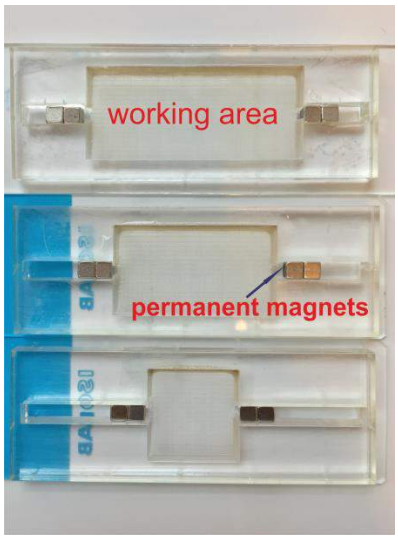

Figure 3.3 Magnetic platform

The actual design of the magnetic platform was implemented on a PMMA material as shown in the Figure 3.3 The permanent magnets dimensions being 3 mm x 3 mm, the platform has a magnets holding place of width of 3 mm and depth of 3mm as well as a variable length for holding the magnets. This variable length allows us to stack and adjust a number of magnets according to our choice. The working place where the glass slides holding the magnetic beads will be placed contains the dimensions 2.5 X 16 mm, 2.5 x 28 mm and 2.5 x 36 mm.

3.1 Magnetic Field Characterisation

To understand how the magnetic field behaves in the working area it is of huge importance to take several measurements. Varying some parameters like the length of the working area or the number of magnets at both sides of the working area and have the field response recorded.

Magnetic field characterization was performed both before and after executing the designs. Before executing the designs, the simulations of these scenarios were performed using the FEMM software. After executing the designs measurements were performed using gauss meter. The experimental and simulations results are all explained in the following subsections. Figure 3.1.1 shows the setup stages for all the experimental work in this section.

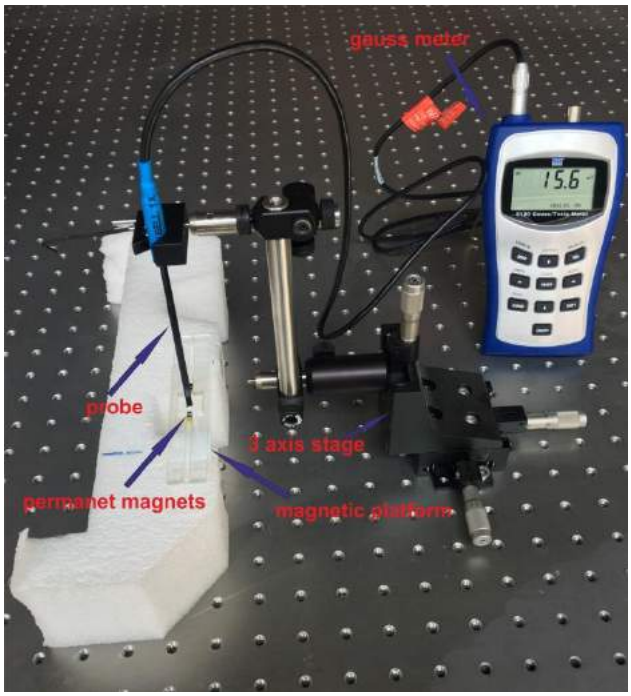

Figure 3.1.1 Complete Setup for magnetic fields characterization

3.1.1 Change in Magnetic Field with Number of Magnets

The working area was designed to have the distance between the magnets at both sides of 15mm. Permanent magnets pairs were then added one at each sides at the same time. Using the gauss meter's measuring tip the field at 7.5mm from both magnets was measured. This field is recorded using the gauss meter's probe for different number of magnets at exactly the same place of the working area for every increase in the magnets. This same scenario was also simulated using the FEMM software before actual execution of the design.

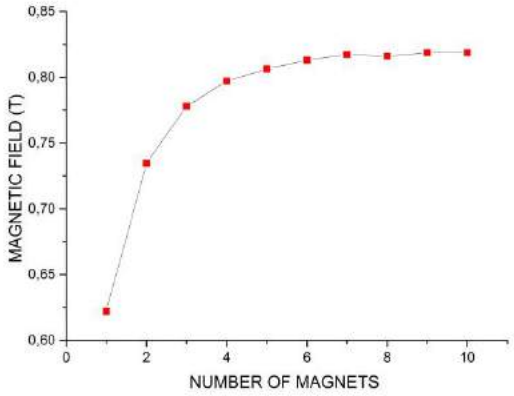

Figure 3.1.1.1 Simulation results for the change in magnetic field against the number of magnets

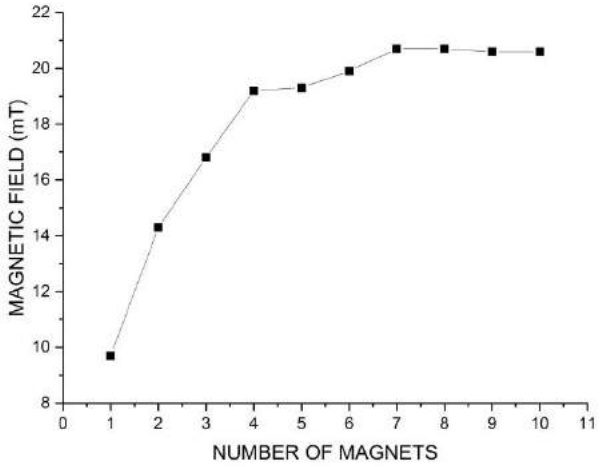

Figure 3.1.1.2 Experimental results for the change in magnetic field against the number of magnets

Shown in Figure 3.1.1.1 and Figure 3.1.1.2 are the graphs of the simulation and experimental data respectively. The increase in number of magnets causes an increase in the magnetic field that was measured at the center of the magnetic platform. Stacking magnets that have the same together vertically with opposite poles facing each other at each side of the magnet platform caused a sharp increase only up to four magnets at each side. The relationship seen is the magnetic field at the center increased as the number of magnets. The magnetic field observed by having four magnets at each side if approximately four times that observed by having one individual magnet at each side in the experimental data graph. After that the increase is very small and heading to saturation. At this point further increase only causes a small or no increase in the magnetic field at the center of the platform.

3.1.2 Change in Magnetic Field with the Size of the Working Area

The aim of this experiment was to determine the suitable size of the working area as well as finding another technique to change the magnetic fields in the working area. Basically the change of the magnetic field with the change in the distance between the magnets is observed. Two magnets ware placed on both sides of the magnetic platform and have the change in the field observed by varying the distance between the magnets. The distances observed were 16 mm, 28 mm and 36 mm. These distances were dubbed as platform 0, platform 1 and platform 2 respectively. FEMM software was used for simulation and gauss meter's tip was again used to obtain the measurements. The measurements were recorded at exactly the center points of the platforms.

Figure 3.1.2.1 and Figure 3.1.2.2 shows the simulation results from FEMM software and experimental data obtained using a gauss meter respectively. Platform 0 which has the has a shortest distance of separation between magnets provided high magnetic field measured at the center of the platform compared to Platform 1 and Platform 2 with the former providing more magnetic field than the later. The magnetic field is strong when the magnets are closer together and get weaker when they are far apart.

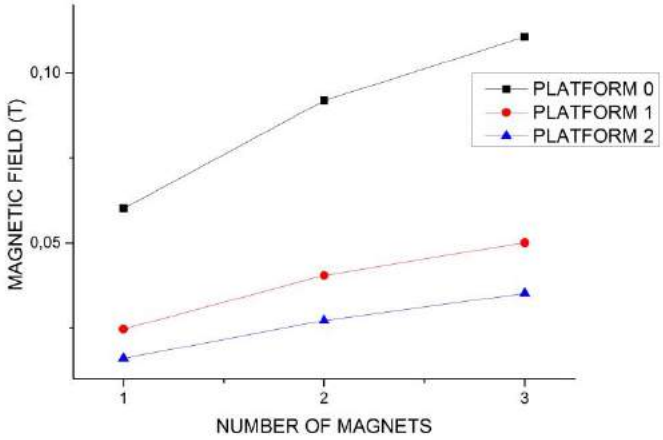

Figure 3.1.2.1 Simulation results for magnetic field change against distance between the magnets

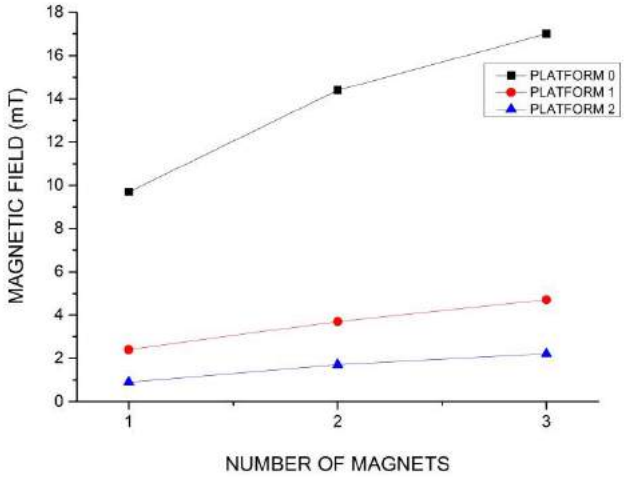

Figure 3.1.2.2 Experimental results for magnetic field change against distance between the magnets

High values of magnetic field were obtained from the simulation software. Small values were obtained upon taking the measurements using the gauss meter. Using the same distance between the magnets and number of magnets, the highest magnetic field values obtained from both simulation and gauss meter are 0.11 T and 17 mT. The

reason for this discrepancy might be due to the faults in calculations, since FEMM software is a free and a simple simulation tool for such problems. However regardless of the discrepancy in the values, both simulation and measured valued showed a similar trend. The increase in the magnetic field at the center of the platform as the distance of separation decreases as well as upon adding the number of magnets at both sides of the platform.

By varying both the distance of separation between the magnets and varying the number of magnets at both sides different values of magnetic fields can be obtained. This option proved to be useful throughout this work as some of the experiments in the following sections required the use of different magnetic fields that could not be provided by only changing the number of the magnets and the length of the working area alone.

3.1.3 Change In Magnetic Field Across The Working Area

Using the gauss meter's tip the magnetic platform was hold still in place with 2 magnets placed in the magnetic field holder. The length of the working area chosen was 16 mm. At exactly the center, the gauss meter's probe was moved sideways across the direction of the magnetic field keeping the same distance away from the magnets. The measurements were taken. The measurements taken were aimed at giving an idea of the width at which the magnetic field is uniform. This will give a good approximation on the size of the magnetic beads containing drop.

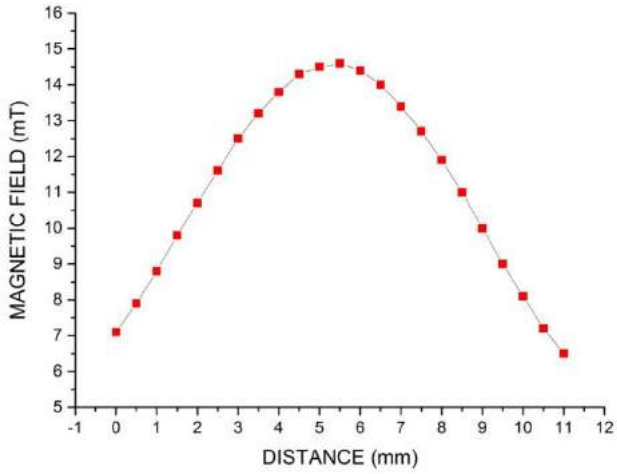

Figure 3.1.3.1 Experimental results showing the variation of the magnetic field across the working area

Figure 3.1.3.1 shows the variation of the magnetic field on the working area across the magnetic platform plotted at an interval of 0 mm to 11 mm. Generally the increase in magnetic field is observed as the probe of the gauss meter is moved towards the center of the platform and a decrease was observed again as the probe is moved away from the center at specific intervals. The global maximum is observed when the probe is exactly at the center of the magnetic platform when the magnets at both ends are directly facing each other. The highest magnetic fields and small changes observed between 3.5 mm and 7 mm are due to the fact the permanent magnets' dimensions being 3 mm x 3 mm x 3mm the magnetic field lines that comes from one pole to another opposite pole at the opposite end are concentrated in an interval of 3 mm at the center and less packed away from this distance.

3.1.4 Change in Magnetic Field along the Working Area in the Direction of the Magnetic Field

The change in magnetic field along the working area of the magnetic platform designed. The length of the working area chosen was 16 mm. At one side of the working area the gauss meter's probe was moved along the direction of the magnetic field across of the working area.

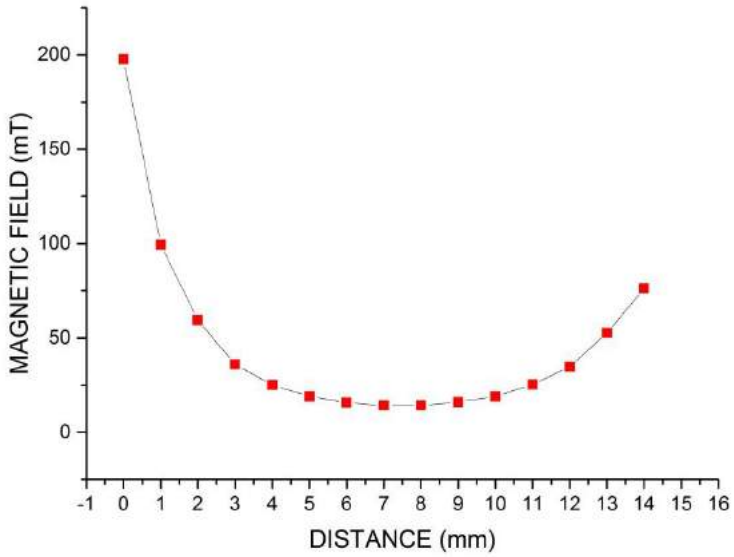

Figure 3.1.4.1 Experimental results showing the variation of magnetic field across the working area

Figure 3.1.4.1 shows the change of the magnetic field in the working area along the direction of the magnetic field. A magnetic field of nearly 200 mT was recorded at distance zero. As the probe was moved towards the other end of the magnetic platform's working area at specific distance intervals, the magnetic field is seen to be decreasing and rising again as the probe gets near to the other end. A fast decrease in magnetic field is observed from 0 mm to 2.5 mm distance. At 2.5 mm from the zero going to 12 mm the magnetic decrease and increase is very small. The magnetic field is more or less constant at this interval. The global minimum is also observed at this interval. This suggests if the magnetic beads are kept between these intervals, they will all be experiencing and magnetized by more or less the same magnetic field.

3.1.5 Change in Magnetic Field along the Depth at the Center of The Working Area

The change in magnetic field along the depth of the magnetic platform was measured with the gauss meter's probe at the center and the depth varied upwards from the bottom at specific interval of 0.5 mm.

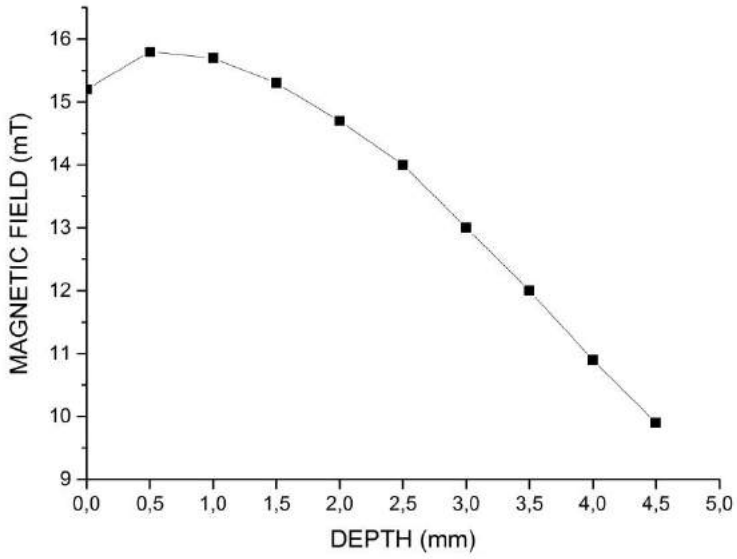

Figure 3.1.5.1 Change in magnetic field with depth at the center

The demonstration of the change of the magnetic field with change in depth at the center of the magnetic platform is shown in Figure 3.1.5.1.The zero depth is at the surface of the platform means the bottom on the surface. The change magnetic fields

plotted are values obtained as the probe was moved from the surface upwards at specific distances up to 4.5 mm above the surface. A maximum of 15.8 mT was recorded at 0.5 mm from the surface suggesting the magnetic field lines are more concentrated at around this region. The magnetic field decreases as the probe was moved upwards. Magnetic fields greater than 12 mT are obtained at the depth less than 3.5 mm.

These results reported in this section provide a very crucial piece on information on how to position the magnetic beads containing glass slides in the platform. If all the parts of the magnet beads containing drop on top of the glass slide placed on the platform are to experience a more or less magnetic field then they should be positioned at the center of the magnetic platform. Also the size of the drop should be about 3 mm diameter and about 4.5 mm in height. Taking these values into consideration a 4 μL total volume of drop of magnetic beads as used in the following experiments fell under these specifications. Thus it is safe to say that all the magnetic beads will experience the same magnetic field.

3.2 Flow Chamber Design and Magnetic Field Characterisation

A flow chamber to be use in fluid flow experiments in this was designed. It was designed using two layers of PMMA material and glass slide as shown in Figure 3.2.1 . This cut PMMA material were then glued together to form a complete packed flow channel. The dimensions of the chamber were 45 mm x 4 mm x 1.5 mm. The top of the flow chamber contain two holes which are used as inlets and outlets connected to syringe pumps (New Era Pump system, NY). The flow chamber also contains a place where permanent magnets that will be used to provide the required magnetic field for amplification process will be placed.

The magnetic field of the flow chamber was also measured by using gauss meter's probe. Two permanent magnets were placed at each side of the magnetic beads as shown in the picture above and the magnetic field was measured and plotted along the direction of the flow.

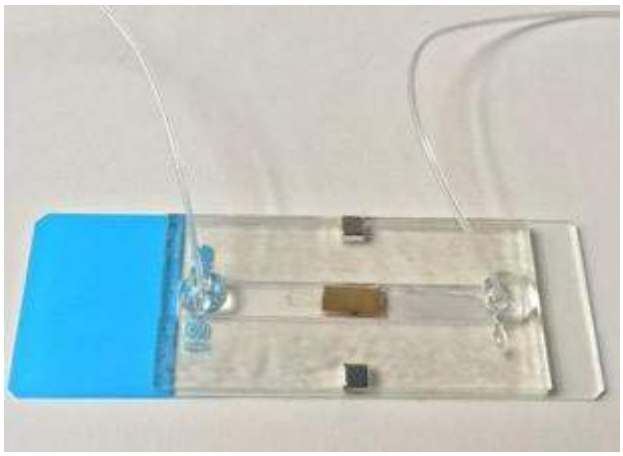

Figure 3.2.1 Flow chamber

Figure 3.2.2 shows the graph of the measured magnetic field along the direction of fluid flow in the flow chamber as measured by the gauss meter's probe. Throughout the flow chamber there seem to be a magnetic field of small magnitude. The magnetic field increases from one end of the flow chamber towards the center and decreases again towards the other end. The global maximum of the magnetic field is expected to be at exactly the center of the flow chamber and the graph should have a Gaussian profile look. The interval at which the measurements of the magnetic field were taken is 0.5 mm. For this reason, the profile is not exactly as expected but it is enough to give the information of the nature of the magnetic field in the flow chamber. The two main important points deducted from the graph are, at any point along the magnetic field is never zero and the highest magnetic field is at the center of the flow chamber. The positioning of the gold-coated glass slides inside the chamber is influenced by this information. In all of the experiments done using this flow chamber design, the magnetic beads containing gold-coated slides are placed at the center of the flow channel so that the magnetic beads experience the highest magnetic field. The magnetic field of around 8.5 mT is achieved at the center.

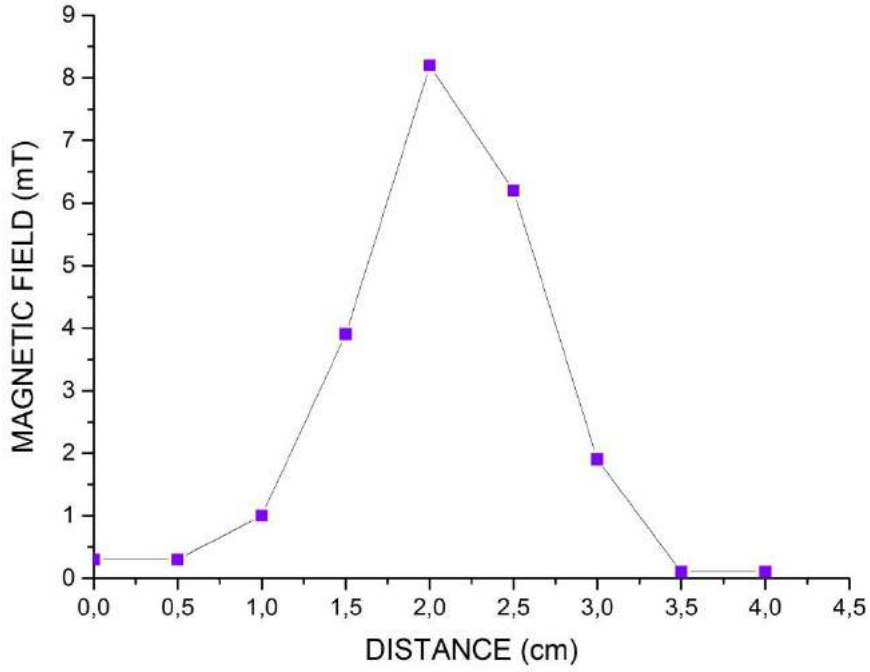

Figure 3.2.2 Magnetic field change across the flow chamber

Chapter 4

Accumulation Dynamics

In this chapter the mechanism, theoretical background of the magnetic beads accumulation based signal amplification method as well as experimental results as explained in [70] are presented. The possibility of using this method to detect important targets such as E.coli bacteria is also shown in this chapter.

4.1 Preparations of the Magnetic Beads and Iron Nanoparticles Solutions

For magnetic bead solution made from ferromagnetic beads or paramagnetic beads (Spherotech) used in these experiments the same concentration of solution was prepared. To prepare these solutions, washing is first done by taking 10 μL of 1.0% w/v from each solution and put in a 1.5 mL capacity micro centrifuge tubes. A suitable amount of PBS was added into the micro centrifuge tubes. Then the microcentrifuge tube is vortexed at 1500 rpm for couple of seconds. After vortexing the tube is kept in a magnetic separator and left to stand there until the solution is clear with the beads accumulated in one side of the microcentrifuge tube where the magnets are situated. This magnetic separation is a standard procedure in the laboratories today. Removal of the PBS solution from the tube was done using a pipette. This removal leaves only the magnetic beads in one side of the tube. This washing process was repeated twice. After the second wash and the removal of the PBS solution only the magnetic beads remained in the tube. 400 μL of PBS was then added into the microcentrifuge tube to make a 0.244 mg/mL magnetic bead solution (pH of 7.4).

For the case of super paramagnetic beads (Chemicell) 2 μL of 10 mg/mL were used, the same procedure was followed in washing twice but later adding 300 μL PBS to make a 0.067 mg/mL solution.

The working concentration of the E.coli 0157 capture beads as reported by the manufacturer is 5 mg/mL. Enough solution of 5mg/mL concentration of these beads was prepared by adding phosphate buffered saline.

Iron nanoparticle solution was prepared by taking a specific amount of concentrated iron nanoparticle solution then PBS was added to make a 0.83 mg/mL solution.

4.2 The Impact of Magnetic Beads Size

To investigate the bead size the following experiments were performed. Custom made glass slides were cleaned and dried. The cleaning was done using ethanol followed by DI water. They were dried using a gentle stream of nitrogen gas. Solutions of 0.244 mg/mL concentration containing three different sizes of ferromagnetic beads and 0.067 mg/mL superparamagnetic beads were prepared using the method explained in earlier section. The sizes were 2 μm, 4 μm and 8 μm and 1 μm respectively. A glass slide was put on the working area of the magnetic platform that has two magnets on each side creating a magnetic field of 12.56 mT at the center of the platform. Using a 2 μL pipette, a drop was of 2 μm beads was put on top of the custom made glass slide. The glass slide together with the drop of the magnetic beads (base beads) was then put inside the working area of the magnetic platform. It's position was adjusted to be at exactly the center of the working area. It is left there to stand for four minutes. During these four minutes the magnetic platform was taken under the microscope objective. After four minutes have passed 2 μL of 1μm superpamagnetic beads (added beads) are pipetted out and added on top of the drop that was being magnetized. Another four minutes are allowed to pass before observing them through the microscope. Pictures were taken for duration of three minutes.

This procedure is again done using different sizes of base beads. The added beads in all the experiments were the same.

The images obtained from these experiments are analyzed using the Nikon NIS software. The lengths of the added beads that form on each single magnetic bead are measure and compared for the different size of the base beads.

From the Equations 2.3.6 and 2.3.7 shows that the magnetic dipole-dipole force has a third order dependency on the dimensions of the beads. The Figure (4.2.1) is the plot of the length of accumulation of the base beads against the size of the base beads. It is seen that the length of accumulation of the added beads increases as the size of the base beads increased.

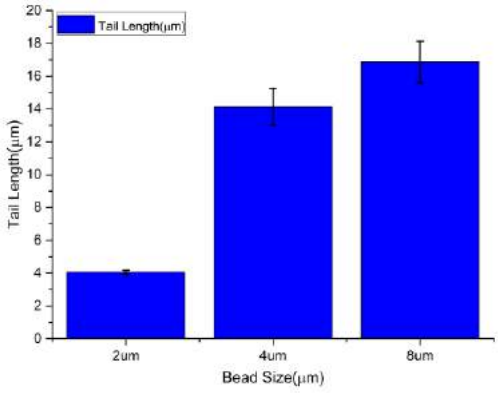

Figure 4.2.1 Impact of magnetic beads' size on the accumulation length

This is an expected trend, as shown in the dipole-dipole force equations that the dipole-dipole force increases as the size of the dipoles involved increases. The increased force causes the base beads to attract more added beads. Magnetic beads with larger sizes create an even larger local magnetic field and attracts more added magnetic beads.

One of the interesting observations made was that the measured length did not match exactly the third order dependency as that which is predicted by the dipole-dipole force equations. This is due to the fact that the dipole-dipole forces given are only the simplified, approximate versions a bid complex equation and that the equations assume an ideal magnetic beads. Although the magnetic dipole-dipole force is of a huge significance in the accumulation, there are other factors that play out too. These factors are the number of the magnetic beads in the surrounding environment, gravity force and the inhomogeneity of the magnetic beads and the liquid. Figure 4.2.2 shows microscopy images showing the different sizes of the base beads and the added beads. From the left are (a) 2 micrometer base bead (b) 4 μm base bead and (c) 8 μm base beads.

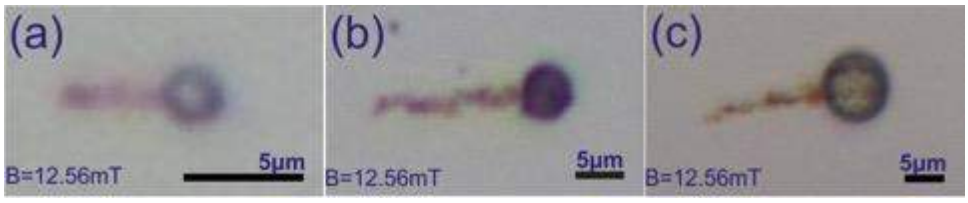

Figure 4.2.2 Microscopy images showing base beads and added bead

4.3 The Impact of the Angle and Distance between the Magnetic Beads on the Magnetic Beads Interaction

To study the impact of θ on dipole-dipole magnetic interaction, ferromagnetic particle pairs having 8 μm, 4 μm and 2 μm sizes were used. On different glass slides pieces containing three permanent magnets at both sides, a 2 μL drop of magnetic particles having 10 mg/ml concentrations was placed and the movements of the particles towards each other under the external magnetic field are video recorded using an optical microscopy system (Nikon). As the droplets of the same magnetic particles' sizes are placed in the magnetic platform, randomly distributed magnetic particles are magnetized and tend to move along the magnetic field. The recorded videos of each magnetic particle size processed offline using the analyze tool (NIS Elements) of the imaging system (Nikon) to reveal the trajectories of magnetic particle pairs. The trajectories are normalized as the stationary particles are at the origin and the trajectories of 21 particle pairs were investigated pair by pair approximately for 20 seconds.

Using the data from the experiment conducted in this subsection, the effect of the distance between magnetic beads on their attraction force was also studied. To quantify this change in distance versus the change in the acceleration of the beads was investigated.

When a same size and randomly distributed magnetic particles containing droplet was placed in the magnetic platform the magnetic particles were magnetized and tend to be aligned along the direction of the magnetic field. The magnitude of the magnetic field is a very important parameter to consider in this case. If the field is high enough to cause translational motion of the formed flocs, the flocs will be attracted away from the center of the drops towards the permanent magnets and accumulate at the edges of the drops. It was observed that at 30 mT this scenario occurred. This is unwanted scenario as the magnetic needed in these experiments should be just enough to magnetize the magnetic beads and cause local movement by dipole-dipole interaction only. The magnetic field observed to fit this case was 15 mT.

However as explained in chapter 2, magnetic force is not the only force acting on the magnetic particles. There are other forces that are acting as well but they were not quantified in this work. The recorded videos of each magnetic particle size are

processed offline using the analyze tool (NIS Elements) of the imaging system (Nikon) to reveal the trajectories of magnetic particle pairs. The trajectories are normalized as the stationary particles are at the origin and the trajectories of 21 particle pairs were investigated pair by pair approximately for 20 seconds.

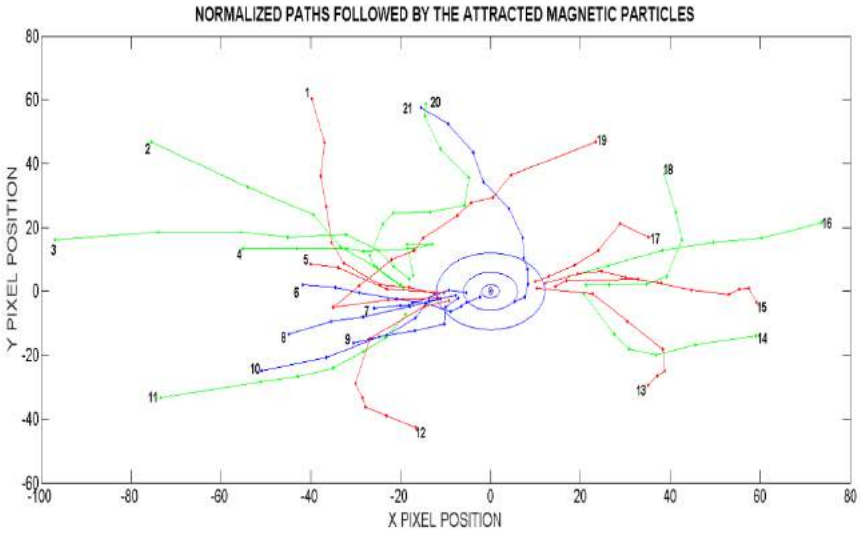

Figure 4.3.1 Normalized paths followed by the attracted magnetic particles

Figure 4.3.1 shows the paths followed by the magnetic particles that were attracted by the stationary particles of different sizes. The stationary particles are shown as circles of different sizes corresponding to the size of the magnetic beads used. Also the trajectories are represented by different colors. The green represents 8 μm, red represents 4 μm and blue represents 2 μm particles' pairs. From the trajectories obtained, it was revealed that the movement of a magnetic bead upon attraction obeyed the Equations 2.3.6 and 2.3.7. Two magnetized magnetic beads followed the direction where θ is approximately 0°. For some particles also the repulsion was also observed at θ of 90° (trajectory 4 and 20). In between these angles the dipole-dipole force can either be attractive or repulsive. Only the effect of θ was investigated in this experiment and it was shown that the direction of the dipole-dipole force is governed by the 1+3 $cos\, 2\theta$ and $sin\, 2\theta$ terms radial and tangential force equations.

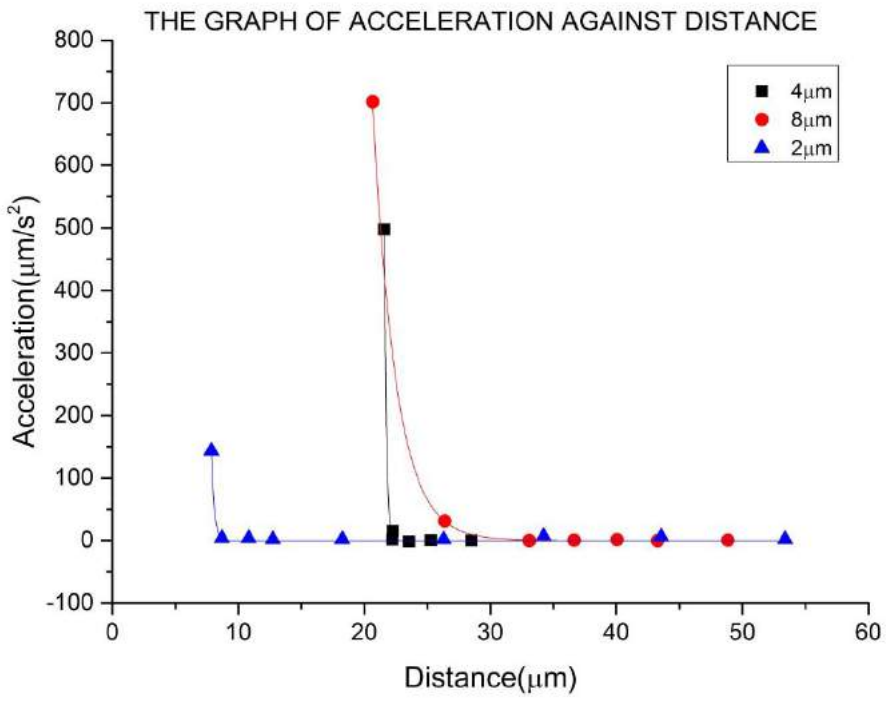

Figure 4.3.2 The change of acceleration of the attracted magnetic beads of different sizes with distance

The figure 4.3.2 shows the change in acceleration against distance between the particles. The acceleration values obtained here can be correlated to the dipole-dipole force. From the Equation 2.3.6 and 2.3.7, the dipole-dipole force is shown to vary inversely as R^4. The dipole- dipole force is expected to be increasing as the distance between the magnetic particles decreases. This is related to the acceleration that will be achieved by the attracted magnetic bead as it gets closer to the stationary bead. The increasing a force of attraction will cause an increase in acceleration of the attracted magnetic bead as it gets closer to the attracted beads. The graph correctly shows this relationship as three magnetic beads' acceleration are shown to be increasing is shown to be increasing and shooting as the particles gets closer to the stationary particle. The maximum acceleration is seen to be decreasing as the size of the beads gets smaller.

4.4 The Impact of Magnetic Field's Strength

In order to investigate the effect of the strength of magnetic field on the accumulation length of the magnetic beads the following experiments were conducted. To study this relationship, two different types of base beads were used. Ferromagnetic

(Spherotech) and paramagnetic (Spherotech), both of mean diameter size 4 μm were used as base beads and superparamagnetic beads (Chemicell) of mean diameter size 1 μm were used as added beads. The same procedure was followed as explained in the subsection 4.2. The same magnetic field was used at each set of experiment and their images taken. The same set of experiments was repeated again only changing the magnetic field. These experiments were done for a couple of different magnetic field values and the images taken for both ferromagnetic (spherotech) and paramagnetic beads (Spherotech).

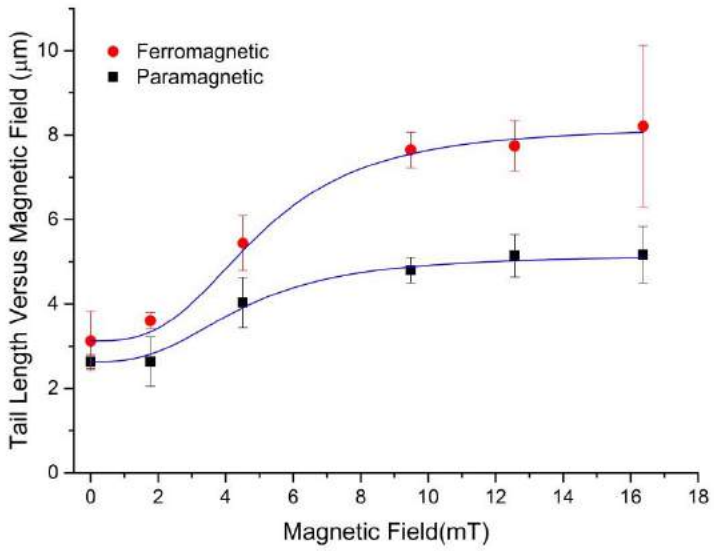

Figure 4.4.1 Accumulation length change against the change of magnetic field for different types of magnetic beads

Ferromagnetic and paramagnetic beads of the same size were used as base beads and the length of the accumulations formed by the added beads at different magnetic field was measured and plotted in Figure 4.4.1.

Generally as the magnetic field was increased the lengths of the accumulation of the added magnetic beads formed increased regardless of the material type of the base beads. As shown by Equations 2.3.6 and 2.3.7 the magnetic dipole-dipole force has a direct proportional relationship with as the square of the magnetic field. Thus the magnetic field increase will cause the magnetic dipole-dipole force to increase. As the dipole-dipole force increases more added beads will be attracted by the base beads forming longer chains than with a lower magnetic field.

However the difference observed between the lengths of the added beads formed on the ferromagnetic beads and paramagnetic beads as the added beads is down to the difference in susceptibilities as explained in the earlier section. Shown is Figure 4.4.2 are the microscopy images of base beads with formed tails of the added beads at different magnetic fields for both ferromagnetic and paramagnetic base beads. From (a)-(c) shows 4 μm ferromagnetic base beads and 1 micrometer added superparamagnetic beads, (d)-(f) shows 4 μm ferromagnetic and 4 μm paramagnetic base beads and 1 μm superparamagnetic added beads.

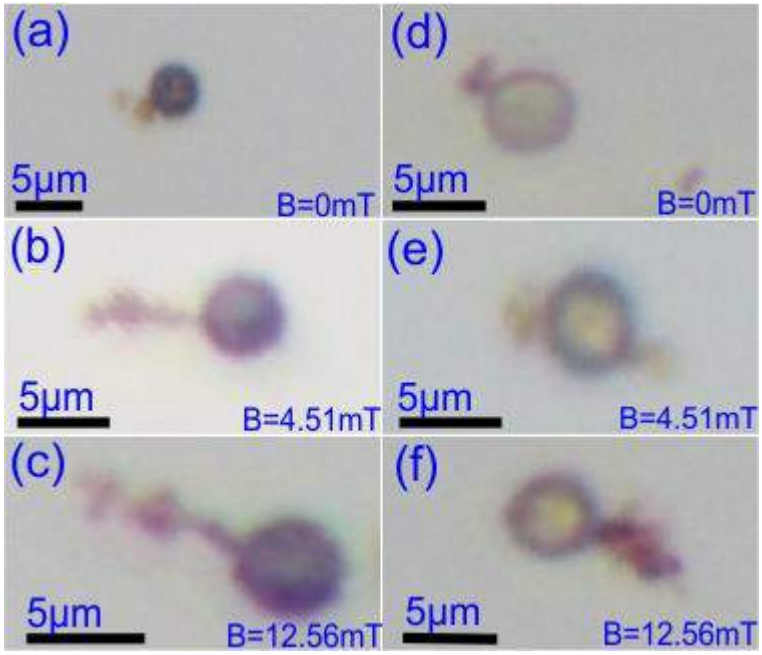

Figure 4.4.2 Optical microscopy images showing the base beads and the added beads at different magnetic field

4.5 The Impact of Magnetic Material Type and Concentration

To investigate the impact of the material type and thus the impact of the magnetic susceptibility and moment the following experiment were conducted. Ferromagnetic beads (Spherotech) and paramagnetic beads (Spherotech) of mean diameter size 4 μm were used and a weak magnetic field of 9.5 mT generated by permanent magnets at the center of the magnetic platform were used. Two different concentration concentrations of ferromagnetic beads were used in this, one 0.244 mg/mL(X1) and the other 0.488 mg/mL (X2). 0.244 mg/mL (X1) of paramagnetic beads were used.

The procedure explained here was applied for the three sets of magnetic beads separately and their images were taken and analyzed. Using 2 μL pipette, a magnetic beads containing drop was put on top of a custom made glass slide placed in the working area of the magnetic platform under the microscope objective. The focus of the microscope was adjusted to give a good view of the magnetic beads inside the drop. The interaction and accumulation of the magnetic beads were observed. Several images were taken at a specific interval for a total duration of six minutes. A number of images were obtained for a single experiment and saved for later analysis. The same procedure was done for the other two sets of magnetic beads.

The lengths of the chains formed in each type and concentration of magnetic beads were measured and compared. The values plotted are are mean ± standard error of the mean, $P<0.05$ for both ferromagnetic concentrations of X1-X2 and ferromagnetic X1- paramagnetic X1. T-test was performed.

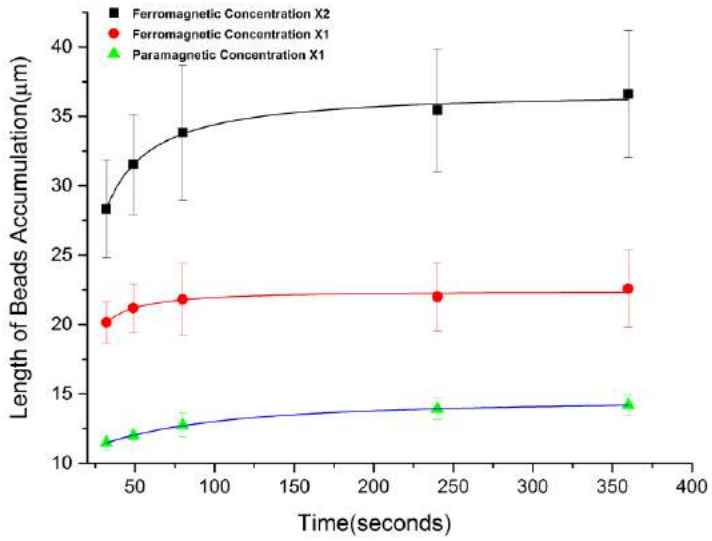

Figure 4.5.1 Experimental results for the change in accumulation length against time

The graph in Figure 4.5.2 shows the average accumulation length obtained at different times. From the graphs it is observed that after 6 minutes the ferromagnetic beads reached an average saturation length of 35 μm for the X2 concentration. For the 1x concentration the average length reached is 22 μm while for the paramagnetic beads the average length reached for 1x concentration is 13 μm.

The formation of longer magnetic bead chains in ferromagnetic beads containing twice concentration X2 Figure 4.5.2 (a) compared to those of concentration X1 Figure

4.5.2 (b) is due to the fact that increasing the magnetic beads concentration increases the number of magnetic beads. Meaning in the same amount of volume used for the X2 concentration contains more number of magnetic beads compared to that of X1. In X2 the ferromagnetic beads are very close to each other compared to X1 ferromagnetic concentration. As shown from the dipole-dipole interaction forces tend to vary as the inverse of distance. Thus the force of attraction or repulsion is the highest when magnetic beads are close to each other. High forces are experienced in X2 concentration thus forming longer chains in a short time compared to that of X1. The longer chains formed in X2 concentration could also produce a higher local magnetic field that can have an effect on close single beads and attract them to form much longer chains. It was also observed that magnetic beads were likely to be attracted by the chains of magnetic beads already formed than to single beads.

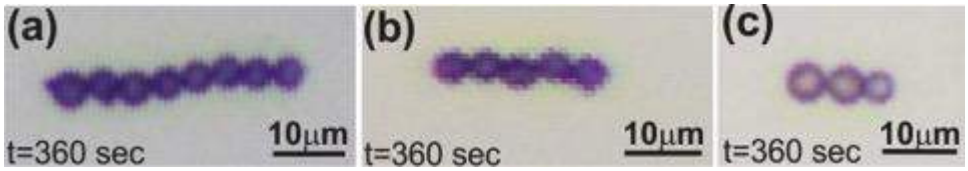

Figure 4.5.2 Microscopy images showing the accumulation of different sizes of magnetic beads at a certain instant of time

To explain the difference between the average length chains formed by the same concentration of paramagnetic beads and that of ferromagnetic beads, larger images of the same sizes around the center points for both ferromagnetic and superparamagnetic beads (Figure 4.5.2 (c)) were taken and the total number of beads were counted for each. The average number of ferromagnetic beads was 575 and that of paramagnetic beads was 655 for the same area size. However longer chains of magnetic beads were observed to be formed on ferromagnetic beads compared to the paramagnetic beads even though the number of paramagnetic beads is higher than that of ferromagnetic beads. Ferromagnetic beads show a tendency of accumulating together to form chains while the paramagnetic beads tend to stay alone forming short chains.

The magnetic susceptibility of ferromagnetic beads is orders of magnitude compared to that of paramagnetic beads. Ferromagnetic beads' magnetic susceptibility is ten times more than that of paramagnetic beads. Magnetic susceptibility measures the degree of magnetization of a material by an external magnetic field. Magnetic field is strengthened by the presence of a more positive of larger susceptibility material. The

magnetic dipole dipole force varies directly as the square of the susceptibility as shown in Equations 2.3.6 and 2.3.7. This is the reason why the response to magnetic field is higher in ferromagnetic beads than in paramagnetic beads and the also why the longer chains are formed by ferromagnetic beads compared to paramagnetic beads.

4.6 The Impact of pH of the Medium

In order to test the performance of magnetic accumulation in liquids with different pH values, hydrofluoric acid and sodium hydroxide were used to prepare DI water solutions having a pH of 2 and 14. Magnetic accumulation in these liquids was investigated following a similar procedure as above. To investigate the impact of pH on the magnetic accumulation, the length of ferromagnetic beads (4 μm) under an applied magnetic field of 9.5 mT was measured and the length after 4 minutes compared to corresponding measurement value in the experiment in Subsection 3.5.4.

After the 4 minutes the lengths of the magnetic beads were measured in both the acidic medium with pH of 2 and in basic medium of pH 4 subjected at a magnetic field of 9.5 mT. It was found that there was no significant difference as the measured valued were all within the standard deviation.

4.7 Iron Nanoparticles Experiments

Iron nanoparticles are cheap; they can respond to magnetic field and can be manufactured with ease. These qualities make them a strong candidate to be used in the place of the added magnetic beads. To demonstrate the feasibility of this statement, the following experiment was done. The goal of the experiment was to show that magnetized particles attract iron nanoparticles and form flocs so that the pixel area of the floc and the bead is increased compared to the pixel area of a single bead under no application of magnetic field.

In this experiment 0.244 mg/mL of ferromagnetic beads (Spherotech) were added on the glass slide on top of the magnetic platform's working area with a 12.5 mT external magnetic field applied. The base beads area left there to stand in the magnetic field for duration of four minutes. After four minutes 2 μL of iron nanopowder solution (0.83 mg/mL) was added onto the magnetized base beads. After four minutes of waiting again, images were taken and analyzed.

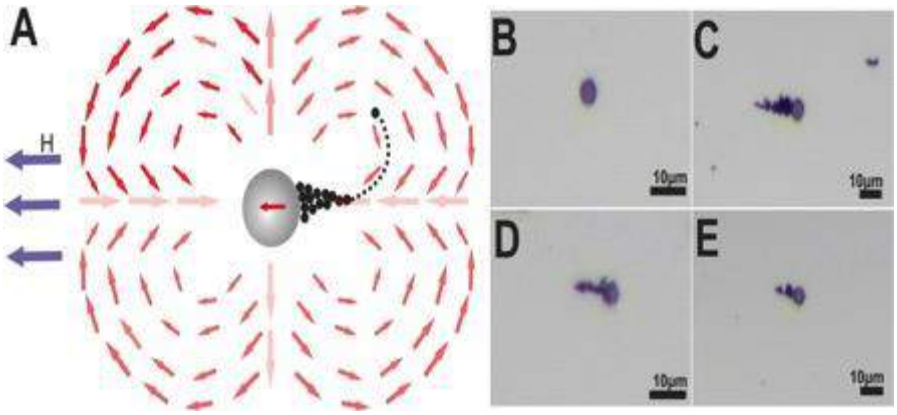

Figure 4.7.1 Accumulation of iron nanoparticles on base beads

The aim of this experiment is to demonstrate the capability of using the method developed in this work as a signal amplification method for 2D images. The main idea is to use the magnetic field controlled flocs to increase the pixel areas of single beads. Upon magnetization of the ferromagnetic base beads local magnetic fields are created by these base beads. When iron nanoparticles (60nm-80nm) are added they are also magnetized, the dipole-dipole interaction forces come into play according to Equations 2.3.6 and 2.3.7. The iron nanoparticles are attracted by the ferromagnetic beads as shown in Figure 4.7.1 A to form flocs around the ferromagnetic beads. Only the flocs that were formed around single beads were quantified. The Figure 4.7.1 (B) is a microscopy image showing a single base bead under no magnetic field, Figures 4.7.1 (C)-(E) shows the accumulation of iron nanoparticle around single ferromagnetic base beads.

The pixel area amplification of approximately two to three folds was achieved by using this method as compared to using just the ferromagnetic beads alone. Area ratios were calculated to obtain these numbers. The average number of the attracted iron particles was also calculated by using area ratios. The area of one single iron nanoparticle was calculated assuming they are ideal spheres occupying a circular area in 2D. The total area of the floc is also calculated assuming the floc is comprised of single layer of iron nanoparticles. Taking the ratio of the total area to that of a single iron nanoparticle, the number of the accumulated iron nanoparticles around a single magnetic bead was found. The number averaged at approximately 7000 iron nanoparticles.

As it has been shown in earlier sections, increasing the magnetic beads and/or the concentration of the added beads techniques can be used to change the length of the

formed chain of added beads around single base beads. These same techniques can also be applied here to increase the number of the iron nanoparticles formed around the single magnetic base beads, thus increasing the pixel area amplification. Figure 4.7.2 are optical microscope images showing an increase in iron nanoparticle flocs obtained by the increase in magnetic field. In this experiments an average of 9000 iron nanoparticles were attracted.

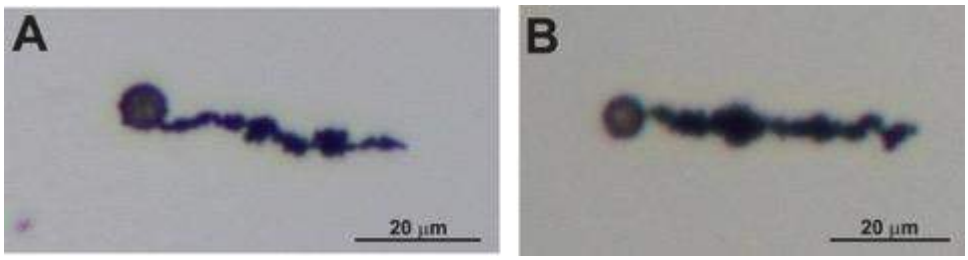

Figure 4.7.2 Microscopy images showing the increase in iron nanoparticle accumulation by increasing the magnetic field

4.8 Combination of Magnetic Separation of E.coli Bacteria and Magnetic Accumulation

E. Coli 0157 is pathogenic and the presence of it in food samples has to be monitored. Conventional immunomagnetic capturing of E. Coli from culture media was performed according to International Organization for Standardization (ISO) E. Coli 0157 detection standard 16654:2001 and a similar procedure can be found in [71].

Briefly E. Coli samples were incubated for 6 hours at 41,5 ^{0}C for pre-enrichment. For immunomagnetic separation 1 mL sample was mixed with 20 μL of magnetic beads, Captivate 0157 (Lab M) coated with anti-E.coli O157 antibodies for 10 minutes. The captured bacteria were separated using magnetic stand, washed and re-suspended in 100 μL in washing phosphate-buffered saline (PBS). Then 40 μL of the solution is transferred to a glass microscope slide and allowed to dry in air. Next, in order to visualize bacteria under optical microscopy and verify that anti-E Coli beads capture the bacteria simple staining by covering the glass slide with crystal violet dye for 1 minute was performed. The excessive dye was rinsed off with water, to complete the standard simple staining procedure. To perform signal amplification, ferromagnetic beads (8 μm) suspended in PBS buffer were added to stained bacteria and permanent magnets were placed on the two sides of the droplet on the glass slide. The anti E. Coli magnetic beads were attracted to ferromagnetic beads as a result of magnetic dipole-dipole

interaction forming an accumulation. The images were then taken and analyzed afterwards. Magnetic separation and the illustration of the signal amplification strategy is shown in Figure 4.8.1.

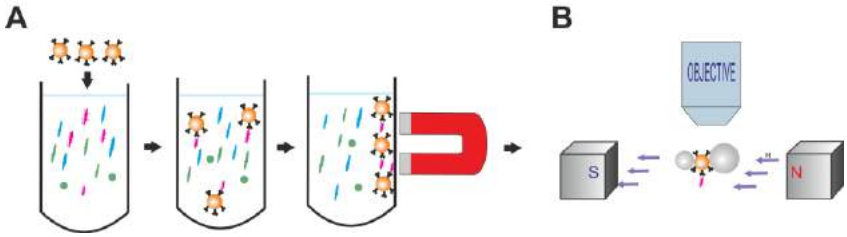

Figure 4.8.1 Illustration of magnetic separation and magnetic accumulation-based amplification

The aim of the experiment is to show that the proposed method in this work can be combined with immunomagnetic separation method and also to provide a proof-of-principle of this method when applied to capture important targets. In this experiment E.coli is our important target. The capturing was realized by using magnetic beads that were coated with anti-E.coli 0157 antibodies. Figure 4.8.2 are microscopy images that show the application of this method on E.coli samples.

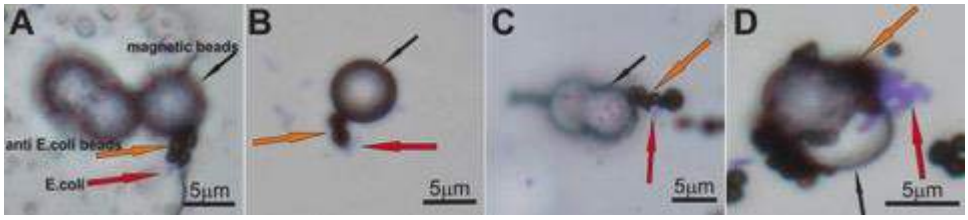

Figure 4.8.2 Optical microscopy images showing the accumulations around E.coli sample

The E.coli samples are stained with violet and pointed by using red arrows, the black arrow shows the ferromagnetic beads and the orange arrow shows the anti-E.coli beads. (A) and (B) shows when the sample is naturally dried and the magnetic field is removed. (B) shows when the sample is wet and under magnetic field, the magnetic beads are observed to align along the magnetic field's direction. (F) Shows many bacteria around magnetic beads indicating non- specific binding is also possible in this demonstration. But it is important to note that the experiment is not a complete demonstration of a sensing mechanism thus no detection limits or specificity studies were performed. In the dry samples, after the removal of the external magnetic field the magnetic beads did not disperse but they stayed coagulated together to form chains as shown. This is due to the fact that some magnetic materials keep their magnetism upon

removal of the external magnetic field. The remaining magnetism is known as residual magnetism.

Staining proved to be very useful for easy visualization of the bacteria and n the calculation o the signal amplification that was achieved in this experiment. Using the imaging system the area of the E.coli bacteria was measured to be 1 μm^2 and that of a single anti-E.coli magnetic bead was measured to be 2.8 μm^2. The dipole-dipole force interaction causes the attraction the magnetic beads with E.coli bacteria captured to be attracted towards the larger magnetic beads as shown in the microscopy images. This accumulation causes an increase in the total pixel area obtained from the area of the magnetic beads and the bacteria compared to using just the bacteria alone. Different flocs were selected and their areas were measured. It was found that the flocs' areas varied from 2.8 μm^2 to 60 μm^2. This corresponded to the minimum amplification of the pixel areas of 3 folds to a maximum of 60 folds. The minımum is contributed by the single anti-E.coli bacteria only. The maximum value is due to the anti-E.coli beads and magnetic beads. The corresponding pixel numbers are shown in Table 4.8.2. For the largest accumulation shown in Figure 4.8.1 A, the number of pixels obtained is 169060.

Single entity	Average number of pixels	Normalized amplification rate
Escherichia coli	1.911	1
Anti-E.coli bead	7.335	3.8
Uncoated magnetic bead	81.51	42.6

Table 4.8.1 Average number of pixel of each entity

Chapter 5

Magnetic Accumulation in A Flow Chamber

5.1 Preparation of Streptavidin, BBSA and BSA Solutions

Different streptavidin solutions were prepared by using a known mass of streptavidin measured from the microbalance and adding a calculated amount of PBS to make a needed molar concentration of streptavidin.

A fixed mass to volume concentration of 2 mg/mL was prepared using specific mass of streptavidin and PBS. The same procedure was repeated to make 1 mg/mL of BSA solution.

5.2 Magnetic Bead Accumulation Around Immobilized Streptavidin Coated Beads

5.2.1 Surface Functionalization of Gold-Coated Slides

This step is aimed at making sure that the streptavidin coated magnetic beads are immobilized on the surface of custom cut gold coated glass slides of size 8.3 x 3.8 mm. Microcontact printing was done using PDMS stamps that contains a 20 μm of alternating lines. The PDMS stamp was made using the procedure explained in [14]. Small pieced of the stamps of reasonable size to be used on the custom cut gold-coated glass slides were cut.

Following this step was the printing of periodic patterns of Biotin-coupled bovine serum albumin (B-BSA) on the gold-coated glass slide. The B-BSA printed will act as a template for immobilizing the streptavidin coated magnetic beads by the biotin-streptavidin interaction. The procedure followed in microcontact printing is as explained in [72]. The PDMS stamps were washed in using ultrasonic cleaner using 70% ethanol and rinsed using 70% ethanol followed by DI water. The stamps were

dried by using a stream of nitrogen gas. The gold-coated glass slides were also cleaned using ethanol and DI water and dried using a stream of nitrogen gas. PDMS stamps were inked with 2 mg/mL of BBSA (Sigma Aldrich). BBSA is left there to stand for 15 minutes before removing the excess solution using a wick of a tissue paper from the stamp. The stamp was again dried using a gentle stream of nitrogen gas. The stamp was brought into contact with the gold-coated glass slide and a small force was applied to make a contact between the two surfaces. This was done for an average of 1 minutes and the stamp was removed afterwards.

The gold-coated glass slide was rinsed gently with PBS to remove the unbound BBSA. Following this step was the blocking of the strips that had no BBSA by using BSA. The gold slides were covered using BSA and incubated for 2 minutes before washing to remove the BSA in DI water. The gold chip containing the BBSA pattern was incubated with streptavidin coated magnetic beads. After 20 minutes of waiting, the gold-coated glass slide was cleaned and dried. The same procedures were repeated using other concentrations of streptavidin coated magnetic beads. The concentrations used were 0.0335 mg/mL, 0.067 mg/mL, 0.67 mg/mL and 6.7 mg/mL. Figure 5.2.1.1 (B) shows the steps followed in this experiment. Part (A) shows the flow chamber viewing under microscope objective.

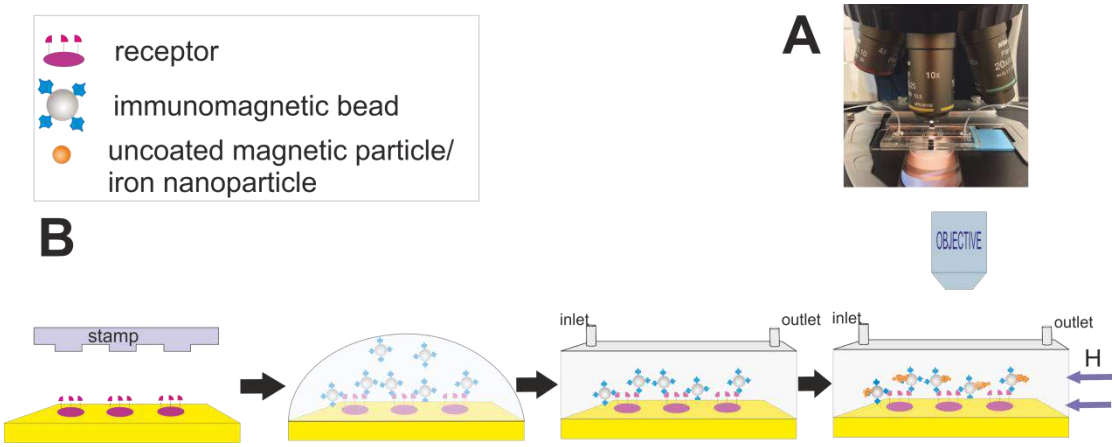

Figure 5.2.1.1 Illustration of the steps of the experiments

The surface chemistry worked well in the experiments. Clear patterns of streptavidin coated magnetic beads were printed on the gold-coated glass slide as seen from the microscope. Figure 5.2.2, the streptavidin coated magnetic beads are printed in lines as shown in the before amplification images (a)-(d).

5.2.2 2D Signal Amplification

The gold-coated glass slides with printed streptavidin coated magnetic beads (base beads) were then placed on the fluidic chamber for signal amplification. Two permanent magnets were placed at both sides of the fluidic chamber. The gold-coated glass slides were placed at exactly the center of the magnetic field where a large field was observed for them to be magnetized. The fluidic chamber was put under the microscope as shown in complete setup Figure 5.2.2.1.

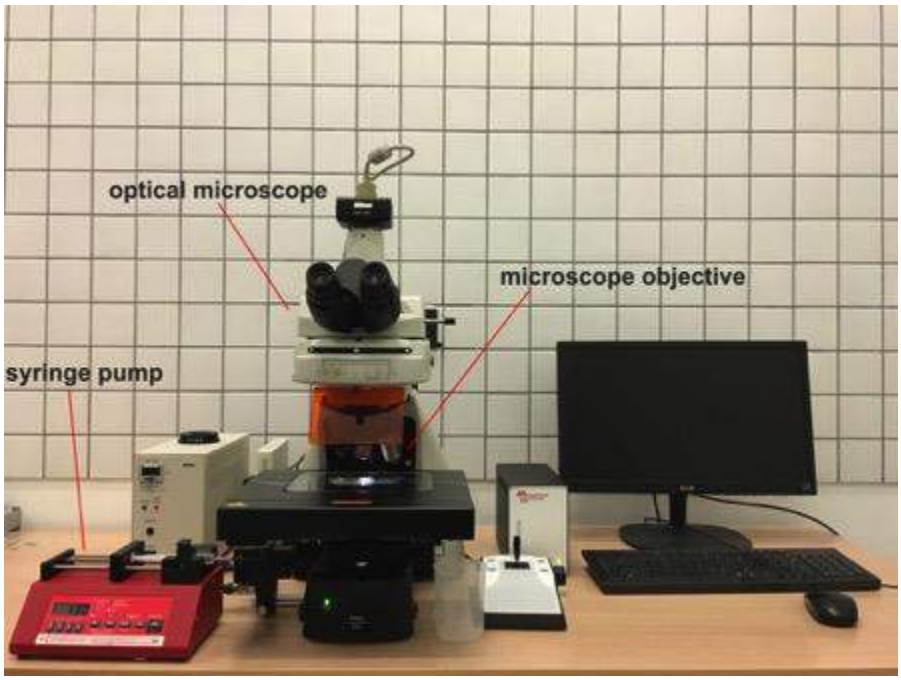

Figure 5.2.2.1 Complete setup of the experiment

Iron nanoparticles were used as the added beads for signal amplification. Iron nanoparticles of concentration 0.25 mg/mL were put in a syringe. Using the inlet tube, the syringe was connected to the fluidic chamber and placed in the microfluidic syringe pump. The iron nanoparticles were pumped to the fluidic chamber at 100 μL /min. The flow was stopped when the fluidic chamber was full.

The interaction of the iron nanoparticles with the printed streptavidin coated magnetic beads was observed and images for both before and after amplification were taken.

This procedure was repeated for the other gold coated glass slides patterned streptavidin loaded magnetic beads at different concentrations of streptavidin.

Inside the flow chamber the magnetic beads are magnetized and when iron nanoparticles solution is allowed to flow in, iron nanoparticles are attracted towards the

immobilized streptavidin beads Figure 5.2.2.2 (e)-(h). The darker accumulations seen in the after images are comprised of iron nanoparticles. They are all aligned towards the direction of the external magnetic beads.

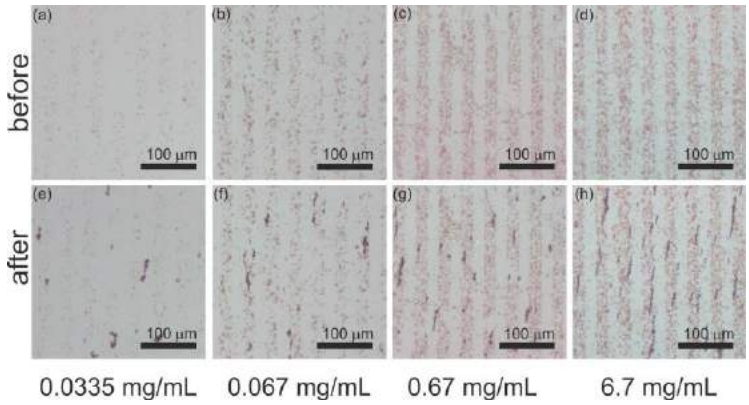

Figure 5.2.2.2 Microscopy images showing the surface of stamped streptavidin coated lines at different concentration for both before and after amplification step

An important observation was made however; during the amplification step it was easier for the incoming iron nanoparticles to be attracted by the already immobilized accumulations of the iron particles that to be attracted by the base streptavidin coated beads. This shows that given a longer time and longer flow times of the iron nanoparticles, longer chains of iron nanoparticles are likely to be formed. Thus both the low rate and the time period at which the iron particles are allowed to flow in are very important parameters. The total time duration the iron nanoparticles were allowed to flow through the flow chamber was 3 minutes. The after images shown in Figure 5.2.2.2 (e)-(h) were taken after this time.

As seen from the microscopy images above that there are other unspecific binding of the streptavidin beads. This issue can be solved by two approaches. 1) Improving the inking of the PDMS stamp, stamping force and drying to make sure that only the intended areas are inked, 2) Improving the washing of the gold-coated glass slides in every step that washing is required.

5.2.3 Quantification of the amplification results.

Increase in pixels' area and Contrast Noise Ratio (CNR) are two metrics that were used to quantify the before and after microscopy images. Shown in the Figure 5.2.3.1

below is the graph showing the increase in pixels against the increase in concentration of the immobilized streptavidin magnetic beads.

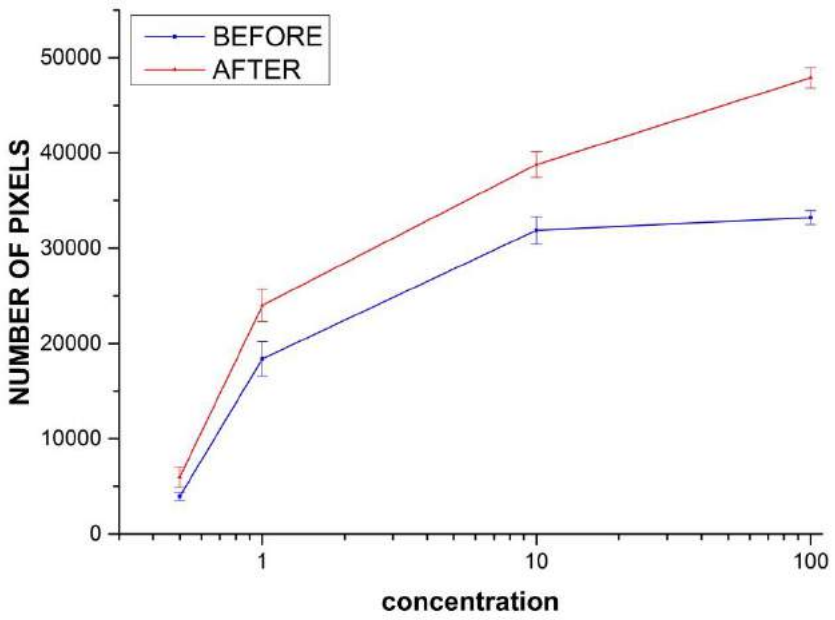

Figure 5.2.3.1 The change in number of pixels due to iron nanoparticles' accumulation

The comparison is made for both before and after amplification. Image thresholding and binary image conversion were two techniques used in finding the total pixels that are occupied by the base magnetic beads before amplification and the total pixels that were occupied by the base magnetic beads + added iron nanoparticles after the signal amplification step. Matlab software was employed in the microscopy image processing

From Figure 5.2.3.1, there is an increase in the pixel area that is occupied by the base beads as the concentration of the base beads is increasing. Also an increase is seen after amplification of the images. The increase in pixel areas shown is due to the attracted iron nanoparticles. From the obtained number of pixels a maximum of 1.4 folds increase in pixels was recorded.

Contrast to Noise Ratio (CNR) is metric that is used to measure the image quality based on contrast between two regions of an image in the region of interest [73]. It is given by the formula below:

$$CNR = \frac{\left|\mu_{object} - \mu_{background}\right|}{\sigma_{background}} \qquad (5.2.3.1)$$

Where μ_{object} is the mean of intensities of the the objects, $\mu_{background}$ is the mean of intensities of the back ground of the image. This value can be converted to decibel form also but in our case it is enough to use this form of the equation. Coding and processing was done using Matlab software.

The profiles of the RGB microscopy images shown in Figure 5.2.3.2 showed that the highest variation in intensities values were shown by the green color pixel compared to blue and red. The profile of the red dotted line in (A) is plotted in (B). Thus green intensity matrix was extracted from the RGB microscopy images and further processing was done using these green intensity values.

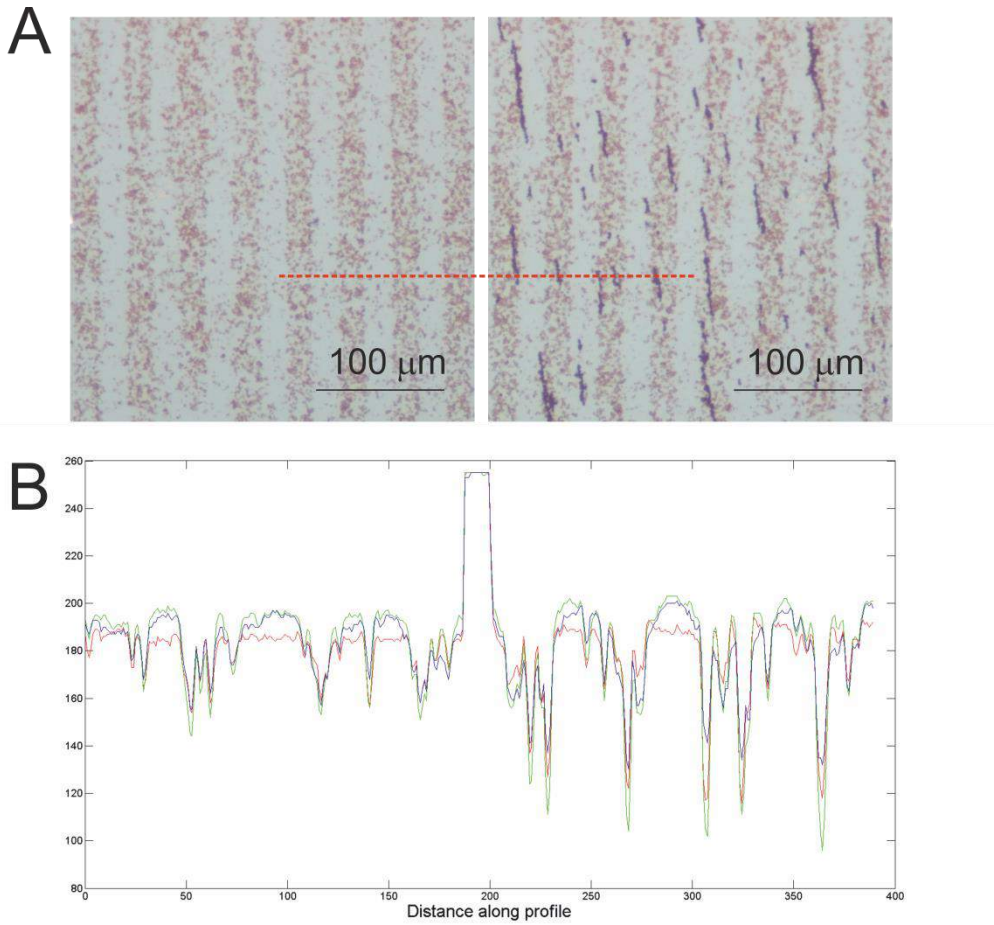

Figure 5.2.3.2 The change in RGB intensity values along the red dotted line

Figure 5.2.3.3 shows the change of CNR values against the increase in the concentration of the streptavidin coated magnetic beads. The CNR increases as the

concentration of the base beads increases. Comparing the CNR of the before microscopy images and after microscopy images, there is an increase observed. A maximum of 6 folds increase is observed as compared to the CNR of the before images.

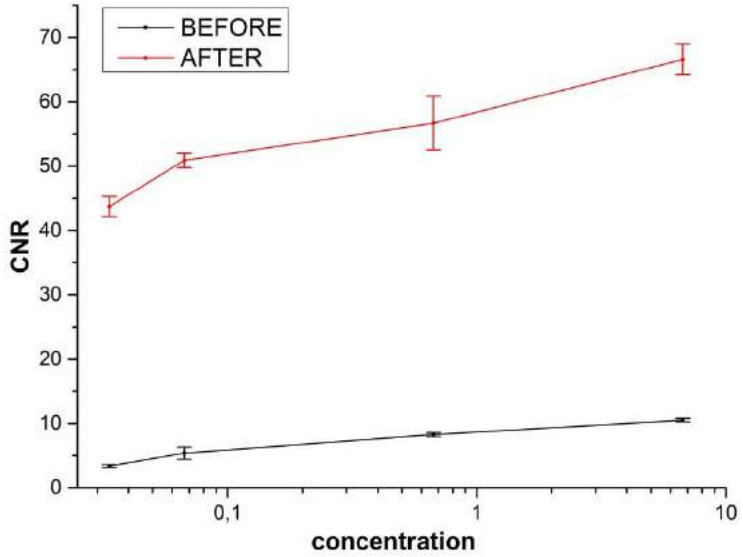

Figure 5.2.3.3 The change in CNR against the change in concentration of magnetic beads

Even though these two metrics used here could show improvements in the obtained images after the amplification step in the flow chamber, CNR showed a big improvement compared to the increase in pixel area. With this in mind, CNR can be selected as the main metric to be used to quantify and show the improvements of the microscopy images obtained from signal amplification method presented in this work.

5.3 A Complete Biosensing and Signal Amplification Procedure

In this work, a complete biosensing strategy was developed. This section is aimed at amplifying 2D-signal of a targeted molecule (streptavidin) using biotin coated magnetic beads by employing the technique of dipole-dipole interaction that has been explained in this work. The flow of the experiments is as shown below in the Figure 5.3.1. Comprising of three steps namely as streptavidin capturing (detection) and magnetic separation, surface functionalization and signal amplification in a flow chamber.

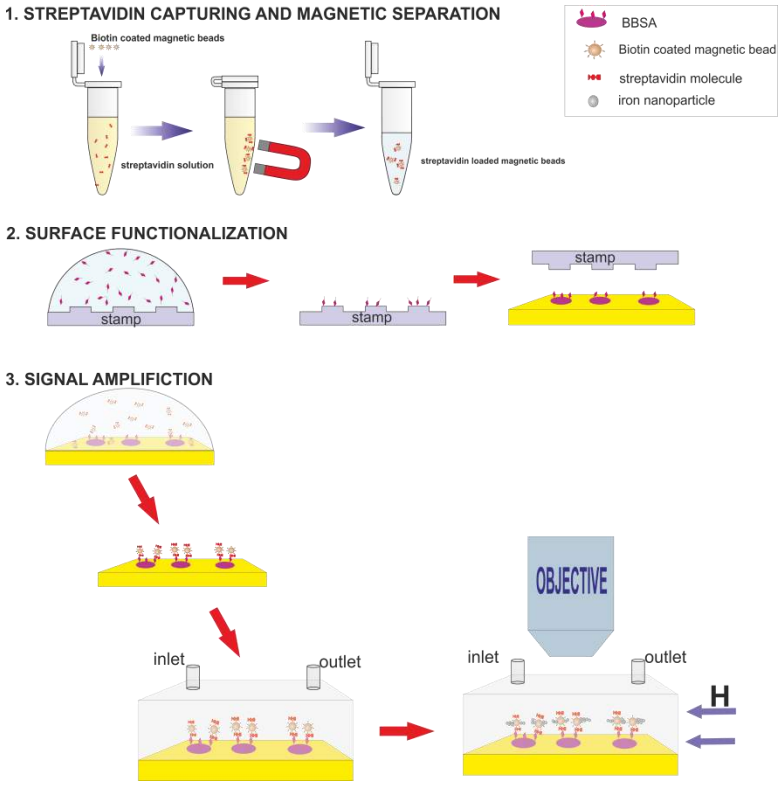

Figure 5.3.1 Schematic for the flow of streptavidin detection experiments

5.3.1 Streptavidin Detection and Magnetic Separation

Streptavidin is known to have a high affinity to biotin. The streptavidin- biotin covalent bond is one of the strongest bonds known. In this subsection streptavidin capturing by using biotin coated magnetic beads and magnetic separation is explained.

Different concentrations of streptavidin were prepared and kept in microcentrifuge tubes. Streptavidin was detected/captured by using biotin coated magnetic beads (Chemicell). From a microcentrifuge tube 25 µL of 100 nM streptavidin were taken and put to another microcentrifuge tube. In the microcentrifuge tube containing 25 µL of streptavidin (Sigma), 35 µL of 100 mg/mL of Biotin coated beads (chemicell) were added. The mixture was then vortexed for 40 minutes at 400 rpm. The microcentrifuge tube was then placed in the magnetic separator and left to stand until all the beads were attracted at one side of the tube and the solution is clear. The clear fluid was then pipetted away and the remaining streptavidin loaded magnetic beads were washed vigorously twice. The washing step was done as explained in [24]. The schematic for this process is as shown in the part 1 of Figure 5.3.1.

5.3.2 Surface Functionalization of the Gold Coated Slides and 2D Signal Amplification

These two steps followed the same procedures that were explained in subsection 5.2.1 and 5.2.2 The only difference here is that the base beads used in the earlier sections were comprised of only streptavidin coated magnetic beads but the ones used here are the biotin coated magnetic beads containing streptavidin (captured target molecule) that was captured by using the procedure explained in subsection 5.3.1 above. The rest of the procedures are as explained in section 5.2.2. The schematic of the process is shown in Figure 5.3.1 part 2 and 3. Viewing under the microscope and quantifying the microscopy images using the MATLAB software followed after the microscopy images were obtained. The three procedures are repeated for different concentrations of streptavidin. The concentrations used were 100 mM, 10 mM and 100 nM.

Figure 5.3.2.1 shows the optical microscopy images obtained before and after amplification step. The before images shows the printed lines of immobilized streptavidin loaded biotin magnetic beads for different concentrations of streptavidin molecules the after images shows the immobilized biotin magnetic beads with iron nanoparticles accumulations.

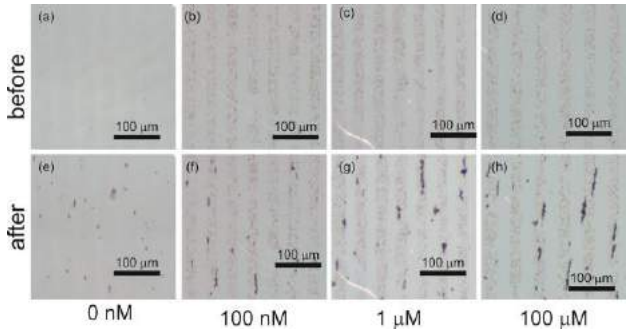

Figure 5.3.2.1 Optical microscopy images showing before and after amplification stage in the flow chamber

Since the gold-coated slides were functionalized with Biotin-Bovine Serum Albumin (BBSA), the adhering of coated magnetic beads proved that our target molecule (streptavidin) was captured. Because the captured streptavidin that is attached to the biotin coated magnetic beads by streptavidin-biotin bond is expected to be form bonds again with the biotin molecules that are on the gold surface from the BBSA.

From subsection 5.3.2, it has been shown that the increase in pixel areas after magnification matric did not show a huge improvement compared to the CNR. Figure (5.3.2.2) shows the CNR values obtained from both before and after amplification against the increase in concentration of streptavidin. A logarithm axis is preferred so as to disperse the values for a clear visualization. A maximum of 8 folds increase in CNR is recorded after the application of the magnetic bead accumulation based signal amplification method developed in this work.

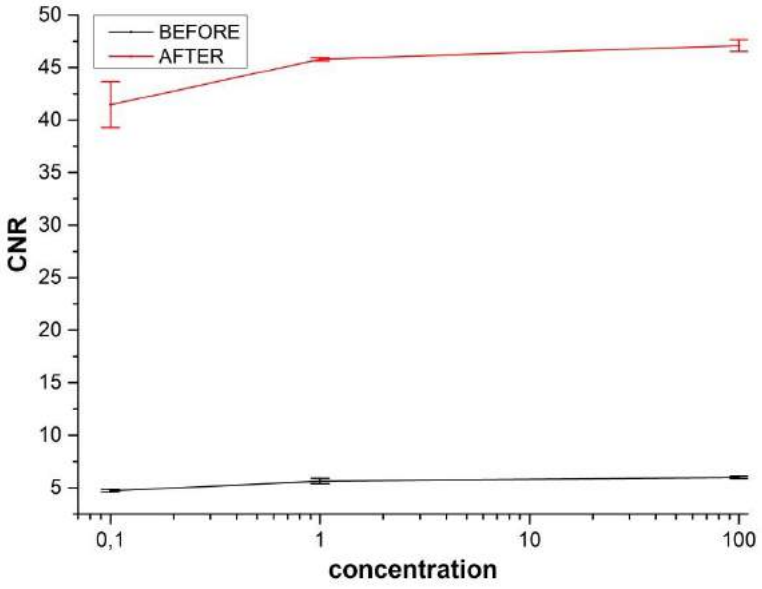

Figure 5.3.2.2 The CNR change with concentration for before and after amplification stage

5.3.3 Specificity Test

To test the specificity of the sensing method described in the earlier section. A control experiment was performed. In the control experiment biotin coated magnetic beads were used but without detection of streptavidin. The beads were not incubated or mixed with the streptavidin solution. After printing BBSA molecules on the gold coated slide and blocking the unprinted area with BSA, biotin bead drops were added on the gold coated glass slides and allowed to stand for the same duration of 20 minutes. After 20 minutes the slides were washed and dried before viewing them under the microscope. The images taken were compared to the images obtained from subsection 5.3.2 of this work.

Then the gold slides were put inside the flow chamber and the same procedure was followed as in section 5.2.2 for amplification. The results obtained were used to test the validity of this method developed in this work.

In Figure 5.3.2.1 (a) and (e), microscopy images containing the results of a control experiment are shown. It is observed that even under no surface base beads, the iron nanoparticles could still form accumulations on top on an empty gold-coated surface. The main working principle involved in the flow chamber experiments, is that the magnetized stamped base beads will provide a platform/template where the added iron nanoparticles will accumulate. In a large magnetic field, the base beads on the surface will create local field lines on the gold-coated surface causing the non-uniformity of the magnetic field on top of the gold-coated slides. The magnetic field is slightly higher in the regions where there are printed base beads. Thus the iron particles instead of settling everywhere, they settle on the lines of the printed magnetic beads. As the iron nanoparticles accumulations grow bigger, more iron nanoparticles are attracted towards the iron nanoparticles accumulations and their lengths grow bigger in size.

This argument was proved numerically by using a simple randomity test developed. The number pixels that are occupied by the iron particles accumulated on the base beads was calculated by simple thresholding technique at a certain triangle 1000 pixels length and 75 pixels width of the stamp and the number of pixels occupied by the iron nanoparticles that have settled in regions with no lines was calculated for a rectangle of the same length and width. Then their differences were taken, and this procedure repeated for another four pairs of rectangles. The average of the total differences was obtained to be 69.05 pixels. During the calculation no negative differences were obtained.

The same procedure calculation is repeated for the microscopy images without base beads. The triangles of the same sizes are chosen as in the above cases. The average of their differences in pixels is calculated. In this attempt the average number of pixels obtained is 1930.65 pixels. During the calculations both negative differences and positive differences were obtained.

These values shows that the iron nanoparticles accumulations formed in the gold-coated slide with no base beads are random. By using this technique it is expected for them to cancel out to give a value close to zero. The fact that no negative differences were obtained in the iron nanoparticles accumulations on the gold-coated slide with

base beads prove that most of the accumulations are on the stamped base beads and thus ordered. This proves the above made explanation that the iron nanoparticles are attracted to the stamped base beads duo to the local magnetic field induced on them. Figure (5.3.3.1) shows the differential number of pixels occupied by the iron nanoparticle for different concentrations of streptavidin calculated.

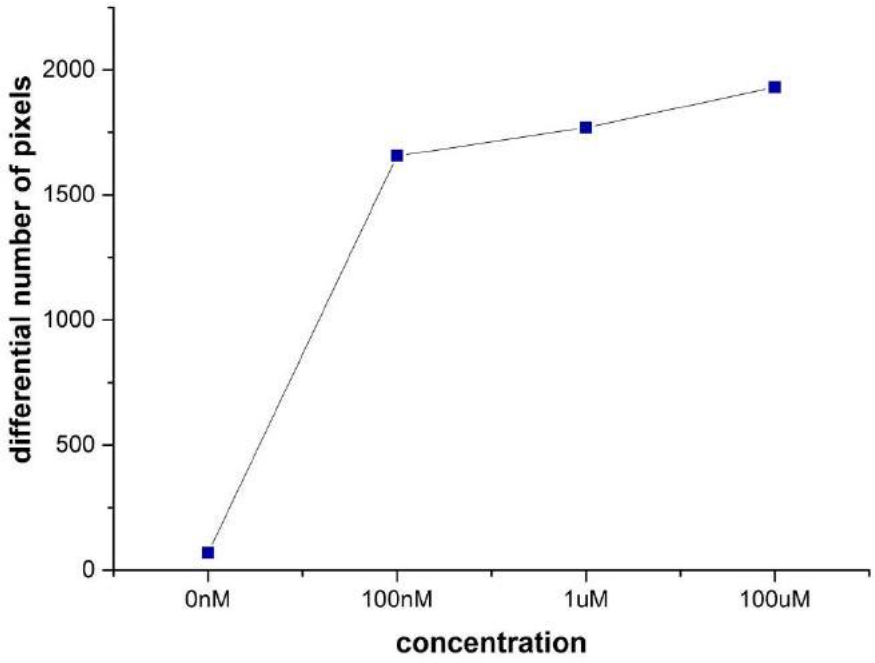

Figure 5.3.3.1 Differential number of pixel of iron nanoparticles against streptavidin concentration

Chapter 6

Conclusion

In this study, a novel cost and time efficient method for signal amplification in biosensors by the use a controlled magnetic or iron micro/nanoparticles accumulation under an external magnetic field has been presented. As the magnetic beads are magnetized they form accumulations that increase in size as the magnitude of the magnetic field or other parameters are varied. This controlled increase in size corresponds to a controlled increase in the pixels occupied and thus pixel amplification is achieved. The accumulation dynamics, the effect of parameters like the magnitude of the magnetic beads, magnetic bead's size and type of the magnetic beads have been investigated.

The integration of this technique with immunomagnetic separation has also been reported. E.coli 0157:H7 bacteria samples were captured by anti-E.Coli magnetic beads and separated from their medium, then magnetic accumulation signal amplification reported in this work was performed. The increase in the total number of pixels was recorded from 1,911 with E.coli only to a maximum of 169,060 with E.coli, anti-E.Coli beads and an accumulation of three magnetic beads. Instead of seeing the capture magnetic bead and E.coli bacteria only the controlled accumulation that are attracted to the capture beads with E.coli bacteria contributed to the increase in pixels reported.

Recently, a lot of microfluidic channel based devices that can detect several diseases with different readout mechanisms have been developed and reported in literature. The integration of this magnetic beads based signal amplification strategy with a flow chamber has also been reported in this work. Signal amplification of the streptavidin coated magnetic beads immobilized on a gold slide inside the flow chamber by the use of iron nanoparticles was quantified. The immobilization of the magnetic beads ensured that the iron nanoparticles area attracted only to the specified regions containing magnetized magnetic beads. Two metrics were used to quantify the micrscopy images obtained. With Contrast to Noise Ratio (CNR) proving an approximate of 6 folds increase compared to a 1.4 folds increase by using the increase in pixel areas metric for both before and after microscopy images.

Lastly, a complete biosensing method that is comprised of the detection of streptavidin molecules, flow chamber integration and signal amplification by the use of iron nanoparticles is reported. A maximum of 8 folds in CNR amplification was obtained. Using empty gold-coated slides without attached base beads a control experiment was done. The quantification results obtained from this control experiment proved that the alignment of the iron nanoparticles on top of the magnetic beads is not random. The iron nanoparticles accumulations are only formed on areas with base beads and are ordered.

With the low cost of the materials used to fabricate the magnetic platforms and flow channels together with not requiring any biomolecular labels, the signal amplification method developed in this work have proven to be cost effeciency. With at most less that 10 minutes needed to achieve complete signal amplification this methods have proven to be time efficiency too. The pH of the medium has no any effect in the accumulations obtained, thus this method can be applied in a media of any pH value.

The use of mobile phone cameras as imaging devices for different biosensors is reported in literature. This magnetic beads accumulation signal amplification method reported in this work can be applied to increase the CNR values or the pixel areas of the images obtained from these devices for better visualization.

BIBLIOGRAPHY

[1] A. Touhami, "Biosensors and Nanobiosensors: Design and Applications," *Nanomedicine*, pp. 374–400, 2015.

[2] P. Mehrotra, "ScienceDirect Biosensors and their applications – A review," *J. Oral Biol. Craniofacial Res.*, no. 2015, pp. 1–7, 2016.

[3] E. B. Bahadir and M. K. Sezgint??rk, "Applications of commercial biosensors in clinical, food, environmental, and biothreat/biowarfare analyses," *Anal. Biochem.*, vol. 478, pp. 107–120, 2015.

[4] L. C. Clark and C. Lyons, "Electrode systems for continuous monitoring in cardiovascular surgery," *Ann. N. Y. Acad. Sci.*, vol. 102, no. 1, pp. 29–45, 1962.

[5] Y. Alapan, K. Icoz, and U. A. Gurkan, "Micro- and nanodevices integrated with biomolecular probes," *Biotechnol. Adv.*, vol. 33, no. 8, pp. 1727–1743, 2015.

[6] A. Koyun, E. Ahlatcıoğlu, and Y. K. İpek, "Biosensors and Their Principles," *A Roadmap Biomed. Eng. Milestones*, pp. 117–142, 2012.

[7] H. Ilkhani, T. Hughes, J. Li, C. J. Zhong, and M. Hepel, "Nanostructured SERS-electrochemical biosensors for testing of anticancer drug interactions with DNA," *Biosens. Bioelectron.*, vol. 80, pp. 257–264, 2016.

[8] M. Pohanka and C. Republic, "Electrochemical biosensors – principles and applications," *Methods*, vol. 6, no. 2, pp. 57–64, 2008.

[9] E. B. Bahadir and M. K. Sezgintürk, "Electrochemical biosensors for hormone analyses," *Biosens. Bioelectron.*, vol. 68, pp. 62–71, 2015.

[10] S. V. Dzyadevych, V. N. Arkhypova, A. P. Soldatkin, A. V. El'skaya, C. Martelet, and N. Jaffrezic-Renault, "Amperometric enzyme biosensors: Past, present and future," *Itbm-Rbm*, vol. 29, no. 2–3, pp. 171–180, 2008.

[11] G. Fadeyev, A. Kalyakin, E. Gorbova, A. Brouzgou, A. Demin, A. Volkov, and P. Tsiakaras, "A simple and low-cost amperometric sensor for measuring H2, CO, and CH4," *Sensors Actuators B Chem.*, vol. 221, pp. 879–883, 2015.

[12] A. Meena and L. Rajendran, "Mathematical modeling of amperometric and potentiometric biosensors and system of non-linear equations - Homotopy perturbation approach," *J. Electroanal. Chem.*, vol. 644, no. 1, pp. 50–59, 2010.

[13] O. O. Soldatkin, V. M. Peshkova, S. V. Dzyadevych, A. P. Soldatkin, N. Jaffrezic-Renault, and A. V. El'skaya, "Novel sucrose three-enzyme conductometric biosensor," *Mater. Sci. Eng. C*, vol. 28, no. 5–6, pp. 959–964, 2008.

[14] J. Lee, K. Icoz, A. Roberts, A. D. Ellington, and C. A. Savran, "Diffractometric detection of proteins using microbead-based rolling circle amplification.," *Anal. Chem.*, vol. 82, no. 1, pp. 197–202, 2010.

[15] Y. H. Zheng, T. C. Hua, D. W. Sun, J. J. Xiao, F. Xu, and F. F. Wang, "Detection of dichlorvos residue by flow injection calorimetric biosensor based on immobilized chicken liver esterase," *J. Food Eng.*, vol. 74, no. 1, pp. 24–29, 2006.

[16] L. Su, L. Zou, C. C. Fong, W. L. Wong, F. Wei, K. Y. Wong, R. S. S. Wu, and M. Yang, "Detection of cancer biomarkers by piezoelectric biosensor using PZT ceramic resonator as the transducer," *Biosens. Bioelectron.*, vol. 46, pp. 155–161, 2013.

[17] V. Perumal and U. Hashim, "Advances in biosensors: Principle, architecture and applications," *J. Appl. Biomed.*, vol. 12, no. 1, pp. 1–15, 2014.

[18] Q. Liu, C. Wu, H. Cai, N. Hu, J. Zhou, and P. Wang, "Cell-Based Biosensors and

Their Application in Biomedicine," 2011.
[19] L. Rotariu, F. Lagarde, N. Jaffrezic-Renault, and C. Bala, "Electrochemical biosensors for fast detection of food contaminants – trends and perspective," *TrAC Trends Anal. Chem.*, 2016.
[20] T. M. Do Prado, M. V. Foguel, L. M. Gon??alves, and M. D. P. T. Sotomayor, "??-Lactamase-based biosensor for the electrochemical determination of benzylpenicillin in milk," *Sensors Actuators, B Chem.*, vol. 210, pp. 254–258, 2015.
[21] World Health Organization, "Global Report on Diabetes," p. 6, 2016.
[22] C.-L. Chang, W. Huang, S. I. Jalal, B.-D. Chan, A. Mahmood, S. Shahda, B. H. O'Neil, D. E. Matei, and C. a. Savran, "Circulating tumor cell detection using a parallel flow micro-aperture chip system," *Lab Chip*, 2015.
[23] C. Chang, S. I. Jalal, W. Huang, A. Mahmood, D. E. Matei, and C. A. Savran, "High-Throughput Immunomagnetic Cell Detection Using a Microaperture Chip System," vol. 14, no. 9, pp. 3008–3013, 2014.
[24] K. Icoz and C. Savran, "Nanomechanical biosensing with immunomagnetic separation," *Appl. Phys. Lett.*, vol. 97, no. 12, p. 123701, 2010.
[25] Z. Altintas, M. Gittens, J. Pocock, and I. E. Tothill, "Biosensors for waterborne viruses: Detection and removal.," *Biochimie*, vol. 115, pp. 144–154, 2015.
[26] X. Wang, P. Zhu, F. Pi, H. Jiang, J. Shao, Y. Zhang, and X. Sun, "A Sensitive and simple macrophage-based electrochemical biosensor for evaluating lipopolysaccharide cytotoxicity of pathogenic bacteria," *Biosens. Bioelectron.*, vol. 81, pp. 349–357, 2016.
[27] I. Lee, W. K. Oh, and J. Jang, "Screen-printed fluorescent sensors for rapid and sensitive anthrax biomarker detection," *J. Hazard. Mater.*, vol. 252–253, pp. 186–191, 2013.
[28] R. Gao, J. Ko, K. Cha, J. Ho Jeon, G. E. Rhie, J. Choi, A. J. deMello, and J. Choo, "Fast and sensitive detection of an anthrax biomarker using SERS-based solenoid microfluidic sensor," *Biosens. Bioelectron.*, vol. 72, pp. 230–236, 2015.
[29] S. H. A. Hassan, S. W. Van Ginkel, M. A. M. Hussein, R. Abskharon, and S.-E. Oh, "Toxicity assessment using different bioassays and microbial biosensors," *Environ. Int.*, vol. 92–93, pp. 106–118, 2016.
[30] Q. a Pankhurst, J. Connolly, S. K. Jones, and J. Dobson, "Applications of magnetic nanoparticles in biomedicine," *J. Phys. D. Appl. Phys.*, vol. 36, no. 13, pp. R167–R181, 2003.
[31] J. Llandro, J. J. Palfreyman, A. Ionescu, and C. H. W. Barnes, "Magnetic biosensor technologies for medical applications: A review," *Medical and Biological Engineering and Computing*, vol. 48, no. 10. pp. 977–998, 2010.
[32] S. P. Gubin, Y. A. Koksharov, G. B. Khomutov, and G. Y. Yurkov, "Magnetic nanoparticles: preparation, structure and properties," *Russ. Chem. Rev.*, vol. 74, no. 6, pp. 489–520, 2005.
[33] L. Vayssières, C. Chanéac, E. Tronc, and J. Jolivet, "Size Tailoring of Magnetite Particles Formed by Aqueous Precipitation: An Example of Thermodynamic Stability of Nanometric Oxide Particles.," *J. Colloid Interface Sci.*, vol. 205, no. 2, pp. 205–212, 1998.
[34] Y. Zhu, H. Da, X. Yang, and Y. Hu, "Preparation and characterization of core-shell monodispersed magnetic silica microspheres," *Colloids Surfaces A Physicochem. Eng. Asp.*, vol. 231, no. 1–3, pp. 123–129, 2003.
[35] X. Liu, J. Xing, Y. Guan, G. Shan, and H. Liu, "Synthesis of amino-silane modified superparamagnetic silica supports and their use for protein

immobilization," *Colloids Surfaces A Physicochem. Eng. Asp.*, vol. 238, no. 1–3, pp. 127–131, 2004.
[36] Y. Zhang, N. Kohler, and M. Zhang, "Surface modification of superparamagnetic magnetite nanoparticles and their intracellular uptake," *Biomaterials*, vol. 23, no. 7, pp. 1553–1561, 2002.
[37] A. H. Lu, E. L. Salabas, and F. Sch??th, "Magnetic nanoparticles: Synthesis, protection, functionalization, and application," *Angew. Chemie - Int. Ed.*, vol. 46, no. 8, pp. 1222–1244, 2007.
[38] M. A. H. Loucha, B. P. Care, and N. Gmbh, "1. Characterization of Microemulsions," pp. 2–5.
[39] G. P. Hatch and R. E. Stelter, "Magnetic design considerations for devices and particles used for biological high-gradient magnetic separation (HGMS) systems," *J. Magn. Magn. Mater.*, vol. 225, no. 1–2, pp. 262–276, 2001.
[40] M. Benz, "Superparamagnetism : Theory and Applications," pp. 1–27, 2012.
[41] C. R. Tamanaha, S. P. Mulvaney, J. C. Rife, and L. J. Whitman, "Magnetic labeling, detection, and system integration," *Biosensors and Bioelectronics*, vol. 24, no. 1. pp. 1–13, 2008.
[42] D. R. Baselt, G. U. Lee, M. Natesan, S. W. Metzger, P. E. Sheehan, and R. J. Colton, "A biosensor based on magnetoresistance technology," *Biosensors and Bioelectronics*, vol. 13, no. 7–8. pp. 731–739, 1998.
[43] F. Li and J. Kosel, "An efficient biosensor made of an electromagnetic trap and a magneto-resistive sensor," *Biosens. Bioelectron.*, vol. 59, pp. 145–150, 2014.
[44] L. Chang, M. Wang, L. Liu, S. Luo, and P. Xiao, "A brief introduction to giant magnetoresistance," 2014.
[45] M. N. Baibich, J. M. Broto, A. Fert, F. N. Van Dau, F. Petroff, P. Eitenne, G. Creuzet, A. Friederich, and J. Chazelas, "Giant magnetoresistance of (001)Fe/(001)Cr magnetic superlattices," *Phys. Rev. Lett.*, vol. 61, no. 21, pp. 2472–2475, 1988.
[46] G. Binasch, P. Gr??nberg, F. Saurenbach, and W. Zinn, "Enhanced magnetoresistance in layered magnetic structures with antiferromagnetic interlayer exchange," *Phys. Rev. B*, vol. 39, no. 7, pp. 4828–4830, 1989.
[47] J. C. Rife, M. M. Miller, P. E. Sheehan, C. R. Tamanaha, M. Tondra, and L. J. Whitman, "Design and performance of GMR sensors for the detection of magnetic microbeads in biosensors," *Sensors Actuators, A Phys.*, vol. 107, no. 3, pp. 209–218, Nov. 2003.
[48] M. D. Angelica and Y. Fong, "NIH Public Access," *October*, vol. 141, no. 4, pp. 520–529, 2008.
[49] W. Shen, B. D. Schrag, M. J. Carter, J. Xie, C. Xu, S. Sun, and G. Xiao, "Detection of DNA labeled with magnetic nanoparticles using MgO-based magnetic tunnel junction sensors," *J. Appl. Phys.*, vol. 103, no. 7, pp. 2008–2010, 2008.
[50] "On a New Action of the Magnet on Electric Currents Author (s): E . H . Hall Source : American Journal of Mathematics , Vol . 2 , No . 3 (Sep ., 1879), pp . 287-292 Published by : The Johns Hopkins University Press Stable URL : http://www.jstor.org/sta," vol. 2, no. 3, pp. 287–292, 2016.
[51] P. A. Besse, G. Boero, M. Demierre, V. Pott, and R. Popovic, "Detection of a single magnetic microbead using a miniaturized silicon Hall sensor," *Appl. Phys. Lett.*, vol. 80, no. 22, pp. 4199–4201, May 2002.
[52] A. A. Bharde, R. Palankar, C. Fritsch, A. Klaver, J. S. Kanger, T. M. Jovin, and D. J. Arndt-Jovin, "Magnetic Nanoparticles as Mediators of Ligand-Free

Activation of EGFR Signaling," *PLoS One*, vol. 8, no. 7, 2013.
[53] B. Da Chan, K. Icoz, R. L. Gieseck, and C. A. Savran, "Selective weighing of individual microparticles using a hybrid micromanipulator-nanomechanical resonator system," *IEEE Sens. J.*, vol. 13, no. 8, pp. 2857–2862, 2013.
[54] A. C. Silva, T. R. Oliveira, J. B. Mamani, S. M. F. Malheiros, L. Malavolta, L. F. Pavon, T. T. Sibov, E. Amaro, A. Tannús, E. L. G. Vidoto, M. J. Martins, R. S. Santos, and L. F. Gamarra, "Application of hyperthermia induced by superparamagnetic iron oxide nanoparticles in glioma treatment.," *Int. J. Nanomedicine*, vol. 6, pp. 591–603, 2011.
[55] P. Fraga García, M. Brammen, M. Wolf, S. Reinlein, M. Freiherr von Roman, and S. Berensmeier, "High-gradient magnetic separation for technical scale protein recovery using low cost magnetic nanoparticles," *Sep. Purif. Technol.*, vol. 150, pp. 29–36, 2015.
[56] L. Dai, Y. Liu, Z. Wang, F. Guo, D. Shi, and B. Zhang, "One-pot facile synthesis of PEGylated superparamagnetic iron oxide nanoparticles for MRI contrast enhancement," *Mater. Sci. Eng. C*, vol. 41, pp. 161–167, 2014.
[57] M. Yamamoto, "Surface Plasmon Resonance (SPR) Theory : Tutorial," *October*, vol. 48, no. February, pp. 1–32, 2008.
[58] T. D. Mai, I. Pereiro, M. Hiraoui, J.-L. Viovy, S. Descroix, M. Taverna, and C. Smadja, "Magneto-immunocapture with on-bead fluorescent labeling of amyloid-β peptides: towards a microfluidized-bed-based operation.," *Analyst*, vol. 140, no. 17, pp. 5891–5900, Jul. 2015.
[59] Z. Cao, Z. Li, Y. Zhao, Y. Song, and J. Lu, "Magnetic bead-based chemiluminescence detection of sequence-specific DNA by using catalytic nucleic acid labels," *Anal. Chim. Acta*, vol. 557, no. 1–2, pp. 152–158, 2006.
[60] L. Liu, S. Wu, F. Jing, H. Zhou, C. Jia, G. Li, H. Cong, Q. Jin, and J. Zhao, "Bead-based microarray immunoassay for lung cancer biomarkers using quantum dots as labels," *Biosens. Bioelectron.*, vol. 80, pp. 300–306, 2016.
[61] X. Xue and E. P. Furlani, "Analysis of the dynamics of magnetic core-shell nanoparticles and self-assembly of crystalline superstructures in gradient fields," *J. Phys. Chem. C*, vol. 119, no. 10, pp. 5714–5726, Mar. 2015.
[62] E. P. Furlani, Y. Sahoo, K. C. Ng, J. C. Wortman, and T. E. Monk, "A model for predicting magnetic particle capture in a microfluidic bioseparator.," *Biomed. Microdevices*, vol. 9, no. 4, pp. 451–63, Aug. 2007.
[63] M. Hejazian, W. Li, and N.-T. Nguyen, "Lab on a chip for continuous-flow magnetic cell separation," *Lab Chip*, vol. 15, no. 4, pp. 959–970, Feb. 2015.
[64] R. Gerber, M. Takayasu, and F. Friedlaender, "Generalization of HGMS theory: The capture of ultra-fine particles," *Magn. IEEE Trans.*, vol. 19, no. 5, pp. 2115–2117, 1983.
[65] A. Bahadorimehr, J. Alvankarian, and B. Y. Majlis, "Magnetic force on a magnetic bead," *2012 10th IEEE Int. Conf. Semicond. Electron.*, pp. 280–284, 2012.
[66] S. S. Shevkoplyas, A. C. Siegel, R. M. Westervelt, M. G. Prentiss, and G. M. Whitesides, "The force acting on a superparamagnetic bead due to an applied magnetic field.," *Lab Chip*, vol. 7, no. 10, pp. 1294–1302, 2007.
[67] M. A. M. Gijs, "Magnetic bead handling on-chip: New opportunities for analytical applications," *Microfluidics and Nanofluidics*, vol. 1, no. 1. pp. 22–40, 2004.
[68] K. W. Yung, P. B. Landecker, and D. D. Villani, "An Analytic Solution for the Force Between Two Magnetic Dipoles," *Magn. Electr. Sep.*, vol. 9, no. 1, pp. 39–

52, 1998.
[69] A. Mehdizadeh, R. Mei, J. F. Klausner, and N. Rahmatian, “Interaction forces between soft magnetic particles in uniform and non-uniform magnetic fields,” *Acta Mech. Sin.*, vol. 26, no. 6, pp. 921–929, 2010.
[70] D. Press, “Magnetic micro / nanoparticle flocculation-based signal amplification for biosensing,” pp. 2619–2631, 2016.
[71] C. Almeida, J. M. Sousa, R. Rocha, L. Cerqueira, S. Fanning, N. F. Azevedo, and M. J. Vieira, “Detection of Escherichia coli O157 by peptide nucleic acid fluorescence in situ hybridization (PNA-FISH) and comparison to a standard culture method.,” *Appl. Environ. Microbiol.*, vol. 79, no. 20, pp. 6293–300, Oct. 2013.
[72] C. L. Chang, G. Acharya, and C. A. Savran, “In situ assembled diffraction grating for biomolecular detection,” *Appl. Phys. Lett.*, vol. 90, no. 23, 2007.
[73] M. Welvaert and Y. Rosseel, “On the definition of signal-to-noise ratio and contrast-to-noise ratio for fMRI data,” *PLoS One*, vol. 8, no. 11, 2013.

Appendix

Appendix A: Materials

Permanent Magnets

3mm x 3mm of size Neodymium (N42) purchased from a local hobby shop.

Poly (methyl methacrylate)/acrylic

Purchased from Mc Master Carr (Elmhurst, IL)

Ferromagnetic Beads

Magnetic beads of reported mean diameter 8.74 μm (5 mL), 4.21 μm (5 mL) and 2 μm (10 mL) were purchased from Spherotech (Lake Forest, IL). Their concentration was 1.0% w/v.

Superparamagnetic beads

Beads of mean diameter size 4.43 μm (10 mL) of concentration 1.0% w/v were purchased from Spherotech (Lake Forest, IL). Beads of mean diameter size 1 μm and concentration 10mg/ml were purchased from Chemicell (Berlin, Germany).

Iron Nanopowder

Iron nanopowder of particle size 60-80 nm in diameter and density 7.86 g/mL at 25 °C was purchased from Sigma-Aldrich (St. Louis, MO).

Gram Stain

Purchased from Merck (Darmstadt, Germany) , was used to color purple the E.coli bacteria for viewing under the microscope.

Captivate 0157 Magnetic Beads.

Beads for capturing E.Coli 0157:H7 were purchased from Lab M (Lancashire, UK). They are coated with high affinity, high avidity absorbed and purified polyclonal antibodies to cell surface antigens.

Sreptavidin (Thermo Scientific)

Purchased from Thermo Fisher Scientific (Waltham, MA). In this work, streptavidin was used in the developing of a complete sensing mechanism as a biological entity to be captured by probe molecules (Biotin) on the magnetic beads.

Biotin Coated Beads (Chemicell)

Beads of mean diameter size 1 μm and concentration 10mg/ml were purchased from Chemicell (Berlin, Germany). These beads were used for specifically capturing streptavidin. Since biotin are known to form a strong covalent bond with streptavidin.

Phosphate Buffered Saline (Pbs)

Purchased from Sigma-Aldrich (St. Louis, MO), PBS was used as a dilution media due to its isotonic property.

Glass Slides

Custom made 8mm x 8mm glass slide made by cutting the pieces from a 25 mm x 75 mm microscope glass slide using laser cutter. The custom made glass slides, served as the basic working area where droplets of magnetic fluids could be placed and observed.

Gold Coated Microscope Slides

Purchased from Sigma-Aldrich (St. Louis, MO). Glass slides coated with 1000-angstrom thick gold.

Biotinylated Bovine Serum Albumin (BBSA)

Purchased from Thermo Fisher Scientific (Waltham, MA). In this work BBSA was used to functionalize gold coated glass slides.

Bovine Serum Albumin

Purchased from Sigma-Aldrich (St. Louis, MO). This was used to block part of the gold surface that had no BBSA on it.

Polydimethylsiloxane (PDMS) Stamps.

These were used to print the patterns of BBSA on custom cut gold coated glass slides.

Hydrofouric acid acid and Sodium Hydroxide

Appendix B: Instrumentation

Optical Microscopy System (Nikon)

In this work the images and videos obtained were recorded using this microscope.

Nikon NIS Elements Software

Analyzing of the images and videos recorded was performed using this analysis tool.

Gauss Meter

Purchased from Pacific Scientific (Milwaukie, Oregon), this device is used to measure the strength and the direction of the magnetic field.

Syringe Pump

Syringe pump was used for pumping magnetic bead solution in and out of the flow chamber. It was purchased from New Era Pumps Inc (NY).

Finite Element Magnetics Method (FEMM V 4.2)

This is free software that is used to solve low frequency electromagnetics problems (both linear and non linear) on axisymmetric domain and two-dimensional planes.